

AD-A281 676



NAVAL POSTGRADUATE SCHOOL Monterey, California



S DTIC
ELECTE
JUL 19 1994
G **D**

THESIS

94-22183



85 PJ

COLD FLOW SIMULATION OF THE ALTERNATE TURBOPUMP
DEVELOPMENT TURBINE OF THE SPACE SHUTTLE MAIN
ENGINE HIGH PRESSURE FUEL TURBOPUMP

By

Richard J. Rutkowski

March 1994

Thesis Advisor:

Garth V. Hobson

Approved for public release; distribution is unlimited

94 7 14 034

Unclassified

Security Classification of this page

REPORT DOCUMENTATION PAGE				
1a Report Security Classification: Unclassified		1b Restrictive Markings		
2a Security Classification Authority		3 Distribution/Availability of Report		
2b Declassification/Downgrading Schedule		Approved for public release; distribution is unlimited.		
4 Performing Organization Report Number(s)		5 Monitoring Organization Report Number(s)		
6a Name of Performing Organization Naval Postgraduate School	6b Office Symbol (if applicable) AA	7a Name of Monitoring Organization Naval Postgraduate School		
6c Address (city, state, and ZIP code) Monterey CA 93943-5000		7b Address (city, state, and ZIP code) Monterey CA 93943-5000		
8a Name of Funding/Sponsoring Organization	6b Office Symbol (if applicable)	9 Procurement Instrument Identification Number		
Address (city, state, and ZIP code)		10 Source of Funding Numbers		
		Program Element No	Project No	Task No Work Unit Accession No
11 Title (include security classification) COLD FLOW SIMULATION OF THE ALTERNATE TURBOPUMP DEVELOPMENT TURBINE OF THE SPACE SHUTTLE MAIN ENGINE HIGH PRESSURE FUEL TURBOPUMP (UNCLASSIFIED)				
12 Personal Author(s) Rutkowski, Richard J.				
13a Type of Report Master's Thesis	13b Time Covered From To	14 Date of Report (year, month, day) March 1994	15 Page Count 85	
16 Supplementary Notation The views expressed in this thesis are those of the author and do not reflect the official policy or position of the Department of Defense or the U.S. Government.				
17 Cosati Codes		18 Subject Terms (continue on reverse if necessary and identify by block number)		
Field	Group	Numerical Simulation, Turbine, Laser Doppler Velocimetry, Space Shuttle Main Engine, High Pressure Fuel Turbopump		
	Subgroup			
19 Abstract (continue on reverse if necessary and identify by block number) Completion of the installation at the Naval Postgraduate School of a cold-flow test facility for the turbine of the Space Shuttle Main Engine High Pressure Fuel Turbopump is reported. The article to be tested is the first stage of the 'Alternate Turbopump Development' model designed and manufactured by Pratt & Whitney. The purpose of the facility is to enable the development of non-intrusive flow measurements and comparison of those measurements with numerical simulations. Flow field characteristics of the turbine stator were predicted using a three-dimensional viscous flow code. A sensitivity study was conducted to determine the effect of inlet profile to flow field solution. Recommendations are made for future use of the test facility and validation of the numerical simulation scheme.				
20 Distribution/Availability of Abstract <input checked="" type="checkbox"/> unclassified/unlimited users <input type="checkbox"/> same as report <input type="checkbox"/> DTIC		21 Abstract Security Classification Unclassified		
22a Name of Responsible Individual Dr. Garth V. Hobson		22b Telephone (include Area Code) (408) 656-2888	22c Office Symbol CODE 31	

DD FORM 1473, 84 MAR

83 APR edition may be used until exhausted

security classification of this page

All other editions are obsolete

Unclassified

Approved for public release; distribution is unlimited.

**Cold Flow Simulation of the Alternate Turbopump Development Turbine of the
Space Shuttle Main Engine High Pressure Fuel Turbopump**

by

**Richard J. Rutkowski
Lieutenant, United States Navy
B.S., United States Naval Academy, 1985**

Submitted in partial fulfillment of the requirements for
the degree of

MASTER OF SCIENCE IN AERONAUTICAL ENGINEERING

from the

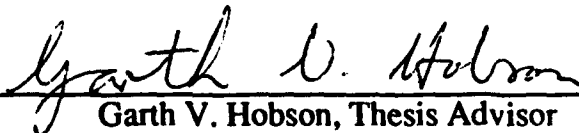
**NAVAL POSTGRADUATE SCHOOL
March 1994**

Author:



Richard J. Rutkowski

Approved by:



Garth V. Hobson, Thesis Advisor



Raymond P. Shreeve, Second Reader



Daniel J. Collins, Chairman,
Department of Aeronautics and Astronautics

ABSTRACT

Completion of the installation at the Naval Postgraduate School of a cold-flow test facility for the turbine of the Space Shuttle Main Engine High Pressure Fuel Turbopump is reported. The article to be tested is the first stage of the 'Alternate Turbopump Development' model designed and manufactured by Pratt & Whitney. The purpose of the facility is to enable the development of non-intrusive flow measurements and comparison of those measurements with numerical simulations. Flow field characteristics of the turbine stator were predicted using a three-dimensional viscous flow code. A sensitivity study was conducted to determine the effect of inlet profile to flow field solution. Recommendations are made for future use of the test facility and validation of the numerical simulation scheme.

Accession For	
NTIS CRA&I	<input checked="" type="checkbox"/>
DTIC TAB	<input type="checkbox"/>
Unannounced	<input type="checkbox"/>
Justification	
By	
Distribution/	
Availability Codes	
Dist	Avail and/or Special
A-1	

TABLE OF CONTENTS

I.	INTRODUCTION	1
A.	PURPOSE	1
B.	OVERVIEW	1
1.	Experiment	3
2.	Numerical Simulation	5
II.	FACILITIES	6
A.	EXISTING TEST CONFIGURATION	6
B.	CONFIGURATION CHANGES	7
1.	Bearings	7
2.	Oil-Mist Cooling System	10
3.	Temperature Monitoring System	10
4.	Vibration Monitoring System	12
5.	Control System	13
6.	Probe Placement	16
III.	EXPERIMENT	17
A.	EXPERIMENTAL PROCEDURE	17
B.	MASS FLOW AND POWER CALCULATIONS	20
IV.	NUMERICAL SIMULATION	22
A.	GRID GENERATION	22

B.	FLOW SOLUTION	24
1.	RVC3D	24
2.	Solution Method	30
V.	RESULTS AND DISCUSSION	33
A.	EXPERIMENT	33
B.	COMPUTATIONAL FLUID DYNAMICS	36
VI.	CONCLUSIONS AND RECOMMENDATIONS	59
A.	EXPERIMENT	59
B.	NUMERICAL SIMULATION	60
APPENDIX A.	ENGINEERING DRAWINGS	61
APPENDIX B.	CALCULATIONS	63
A.	MASS FLOW RATE	63
1.	Flange Taps	64
2.	Vena Contracta Taps	64
B.	TURBINE POWER	65
C.	TURBINE EFFICIENCY	65
APPENDIX C.	COMPLETE TABLE OF MEASUREMENTS	66
APPENDIX D.	FORTRAN PROGRAM AND INPUT FILES	67
LIST OF REFERENCES	74

INITIAL DISTRIBUTION LIST 76

LIST OF FIGURES

Figure 1. Space Shuttle Main Engine	2
Figure 2. Turbine Test Rig	4
Figure 3. Bearing and Shaft Showing Oil Mist Path . . .	9
Figure 4. Oil-Mist Cooling System	11
Figure 5. Stationary Shaft Impact Response	14
Figure 6. Motor-Actuated Rotational Vibration Response	15
Figure 7. Compressed Air System	19
Figure 8. Hub and Endwall Contour	25
Figure 9. C-Grid at Stator Hub	26
Figure 10. C-Grid at Stator Midspan	27
Figure 11. C-Grid at Stator Tip	28
Figure 12. Three-Dimensional Stator Grid	29
Figure 13. General Body-Fitted Coordinate System . . .	31
Figure 14. Specific Power and Mass Flow vs Speed . . .	34
Figure 15. Efficiency vs Speed	35
Figure 16. Low-Speed Vibration Response	37
Figure 17. High-Speed Vibration Response	38
Figure 18. Turbulent Inlet Velocity Profiles	39
Figure 19. Slug-Flow Inlet Velocity Profiles	40
Figure 20. Cray Inlet Velocity Profiles	41
Figure 21. Iris Inlet Velocity Profiles	42
Figure 22. Normalized Pressure - Turbulent	44
Figure 23. Normalized Pressure - Slug Flow	45

Figure 24. Normalized Pressure - Cray	46
Figure 25. Normalized Pressure - Iris	47
Figure 26. Mach Contours - Cray - Turbulent	48
Figure 27. Mach Contours - Cray - Slug Flow	49
Figure 28. Mach Contours - Iris - Turbulent	50
Figure 29. Mach Contours - Iris - Slug Flow	51
Figure 30. Total Pressure - Cray - Turbulent	53
Figure 31. Total Pressure - Cray - Slug Flow	54
Figure 32. Total Pressure - Iris - Turbulent	55
Figure 33. Total Pressure - Iris - Slug Flow	56
Figure 34. Residual History Example	57
Figure A1. Bearing Outer Spacer	61
Figure A2. Probe Mount	62

I. INTRODUCTION

A. PURPOSE

This thesis describes the modification, completion and initial test of a test facility designed to enable the development of non-intrusive measurement techniques within the rotating blade row of a transonic turbine. It also details the computer modeling of a turbine stator flow field for validation of an advanced viscous flow code.

B. OVERVIEW

The performance of a turbomachine depends heavily on the flow fields generated within the machine during its operation. Measurement, prediction and understanding of conditions in the flow field are essential to optimized design of turbomachines. More efficiently cooled blading, enabled by advanced computer modeling and design, can result in significant improvements in service life, reliability and lifecycle cost.

Installation at the Naval Postgraduate School Turbopropulsion Laboratory (TPL) of the cold-flow test facility reported by Studevan [Ref. 1] was completed as part of the present work. The facility was designed to enable tests of a turbine intended to power the High-Pressure Fuel Turbopump (HPFTP) (Fig. 1) of the Space Shuttle Main Engine

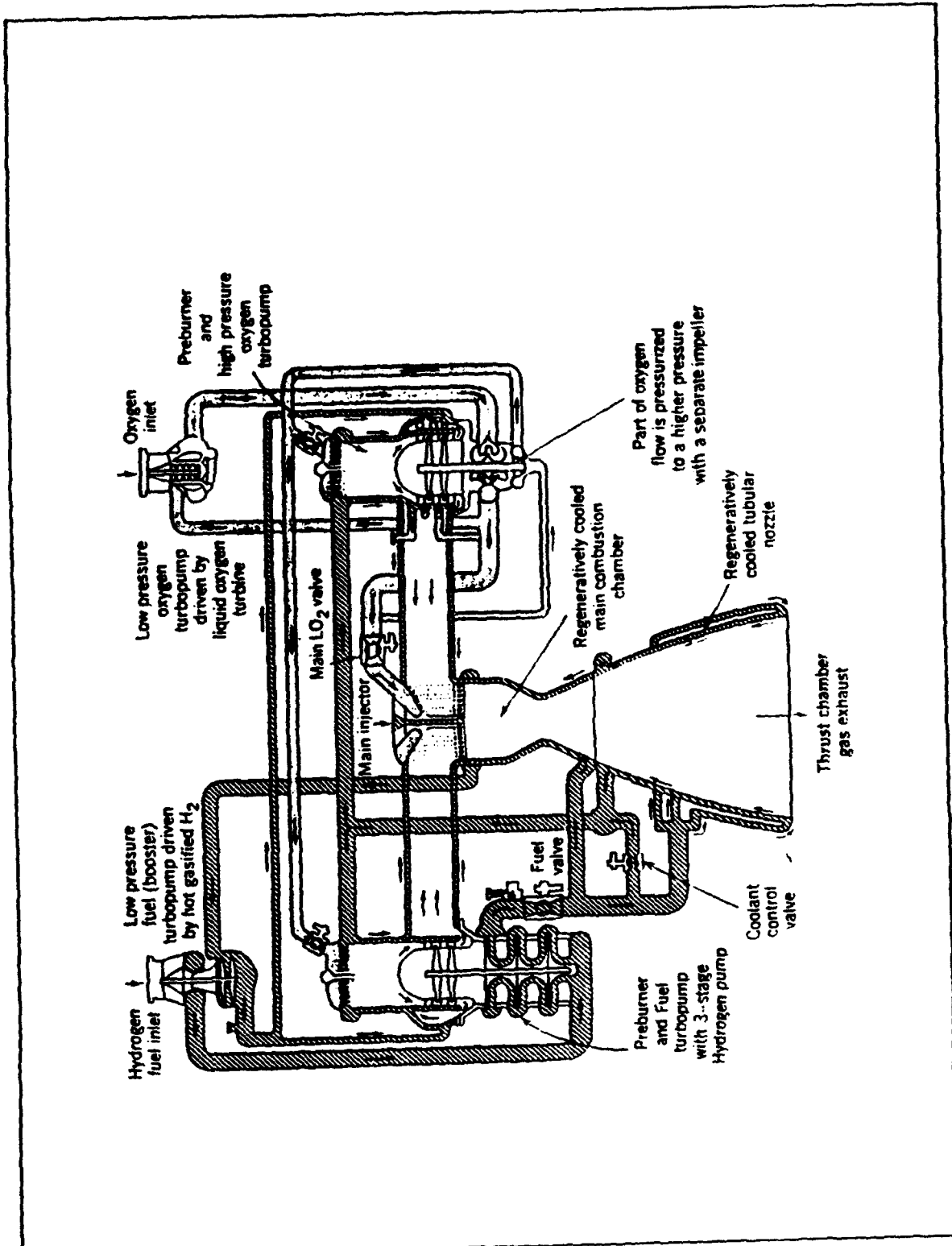


Figure 1. Space Shuttle Main Engine

(SSME). The turbine was designed and manufactured by Pratt & Whitney as the 'Alternate Turbopump Development' (ATD) model.

The purpose of the new Turbine Test Rig (TTR) configuration (Fig. 2) at TPL is to facilitate the advancement of non-intrusive Laser-Doppler Velocimetry (LDV) techniques required to validate viscous flow simulation codes. The long term goal of this research is to use LDV to measure the flow field immediately adjacent to the endwall of the turbine in the tip clearance region. An intermediate goal is to determine the performance of the single, and ultimately the two-stage turbine operating continuously in the TPL facility. Gaddis, Hudson and Johnson [Ref. 2] documented the exit conditions and overall performance of the ATD, while Hudson and others [Ref. 3] investigated the original turbine model. Both of these tests were conducted in a short duration blow-down facility at NASA Marshall Space Flight Center.

1. Experiment

Initial measurements of the ATD will determine the power output of the single stage turbine. The instrumentation documented herein will be primarily that concerned with the safe operation and control of the facility. Provisions have been made for initial flow field testing, which will be made with classical intrusive

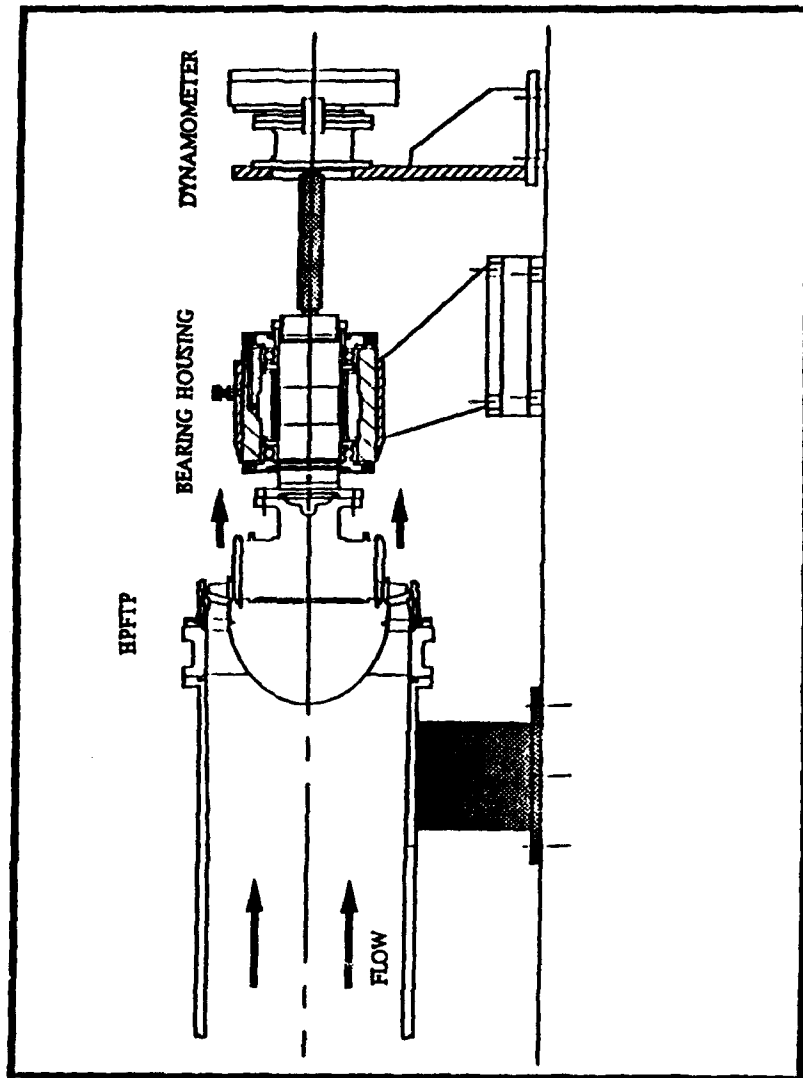


Figure 2. Turbine Test Rig

techniques. The initial tests were conducted to determine the integrity of the turbine and its subsystems.

2. Numerical Simulation

Numerical simulations of the flow field in the first stage stator of the SSME HPFTP turbine were accomplished using two codes developed by Roderick V. Chima called Turbomachinery C-Grid (TCGRID) [Ref. 4], and Rotor Viscous Code 3-D (RVC3D) [Ref. 5]. TCGRID was used for the generation of the 3D volume grid around a single blade element and RVC3D performed the numerical solution of the flowfield.

II. FACILITIES

A. EXISTING TEST CONFIGURATION

The existing configuration of the TTR, as reported by Studevan [Ref. 1], consisted of:

- Inlet Ducting
- ATD
- Shaft and Bearing Housing
- Bearing Housing Support
- Dynamometer
- Bearing Lubrication System
- Controls and Instrumentation.

All of the above listed components are contained within the TTR cell with the exception of the Controls and Instrumentation which are housed in a control room adjacent to the cell. The interior of the TTR cell may be seen from the control room through an explosionproof window. This allows the test rig to be operated and observed from a safe environment. The test arrangement is shown in Figure 2.

During operation, high pressure air flows from the inlet ducting through the inlet strut housing and into the ATD. In the ATD, air passes through the annulus of the first stage stator where it is accelerated and turned off axis. The air then impinges on the first stage rotor blades which

move in reaction to the pressure, turning the rotor disk and converting the energy in the air to rotational energy. The air then exhausts into the TTR cell. As the rotor disk turns, it spins the main shaft in the bearing housing. The main shaft, via the quill shaft, is coupled to the dynamometer where the rotational energy is absorbed.

Shaft speed of the turbine may be sensed and controlled by the dynamometer system. Configuration of the speed control system is unchanged from that reported by Kane [Ref. 6]. Speed may be automatically or manually controlled by adjusting the water flow rate through the dynamometer. In the automatic mode, a magnetic speed-sensor signal is compared to a set point, and a controller drives the difference to zero. The dynamometer is instrumented to provide mechanical power output via torque measurements. The power output may be calculated in two other ways; namely, using the mass flow rate and temperature rise of the water through the dynamometer, or using the mass flow rate and stagnation temperature drop of the air through the turbine.

B. CONFIGURATION CHANGES

1. Bearings

The original design of the shaft and bearing housing called for four high-precision ball-bearing units. After coupling the shaft and bearing housing with the ATD, the

assembly was to be dynamically balanced. Balancing proved to be impossible and the assembly was taken apart for inspection. Upon disassembly, one of the bearing units was found to be damaged. In order to simplify the system, the outer bearing spacer was redesigned so that only two ball bearing units were necessary (Fig. 3). Appendix A contains the engineering drawing.

During reassembly of the shaft and bearing bearing, the shaft was cooled in a refrigerator to 62°F and bearings were slowly heated in an oil bath to 163°F. It was noted that condensation formed on the shaft when it was removed from the refrigerator and it was wiped down prior to inserting the bearing. The shaft was placed on end on a workbench. When the bearing reached the proper temperature, it was removed from the oil bath with tongs and placed on a metal plate. From the plate, it was immediately picked up in gloved hands and carefully but quickly inserted over the shaft. When the bearing was inserted over the shaft in an attitude level with the workbench it did not bind and slid properly into position. The procedure was practiced several times with the damaged bearing before an attempt was made with the actual hardware. To insert the shaft and bearing assembly into the bearing sleeve, the sleeve was preheated on a hot plate to 100°F. The shaft and bearings were then pressed into the bearing sleeve with a milling machine used as a press.

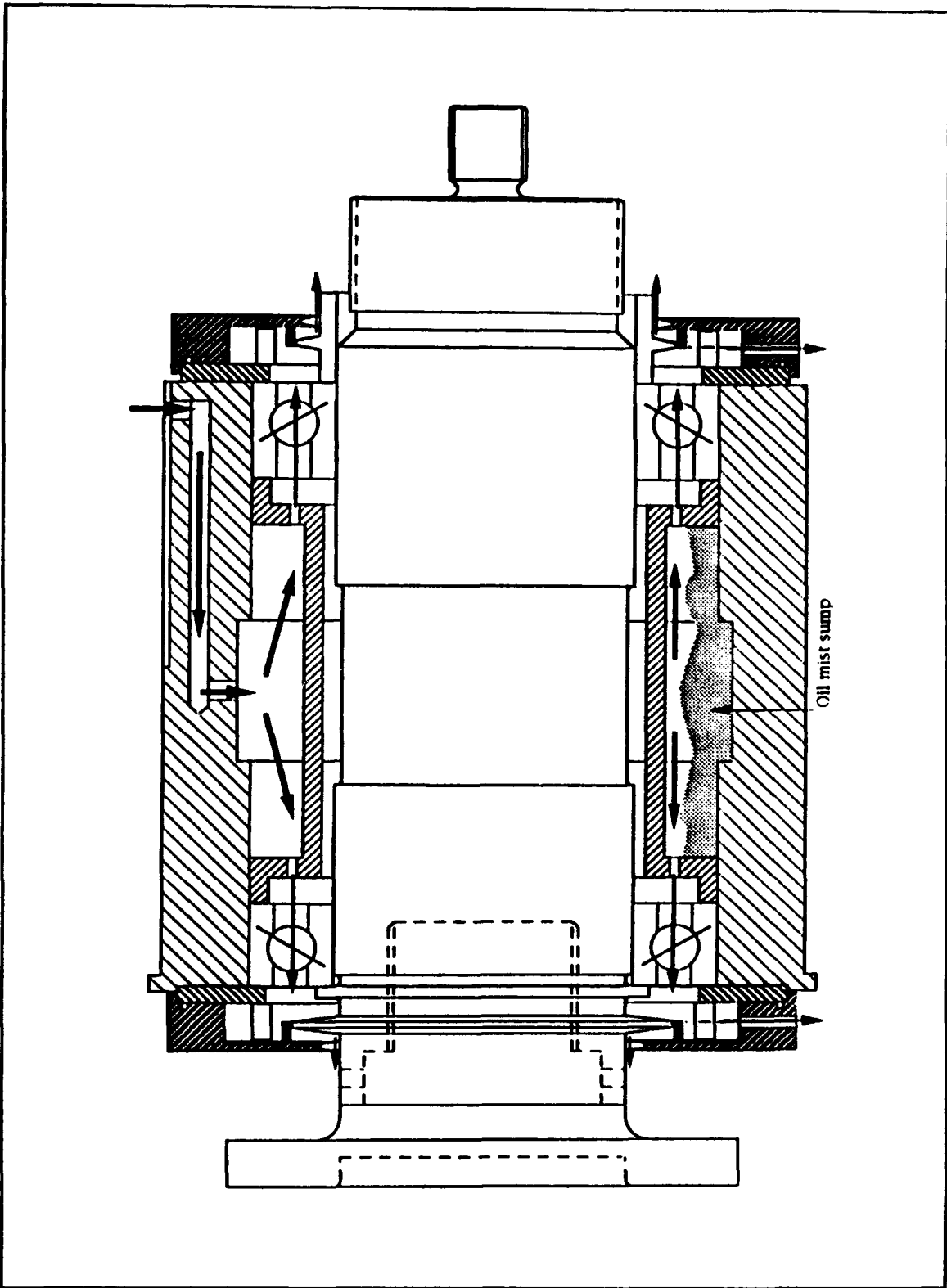


Figure 3. Bearing and Shaft Showing Oil Mist Path

2. Oil-Mist Cooling System

The Portable Turbine Lubrication Unit described by Studevan [Ref. 1] for cooling the high-precision ball bearings was replaced by an oil-mist lubrication system. The system was powered by shop air which passed through a 5 micron filter to remove particulate matter before entering the Norgren Micro-Fog Unit, where it forced a small stream of atomized oil through tubing to a nozzle (Fig. 4). The nozzle was inserted into a hole atop the downstream end of the bearing sleeve (Fig. 3). The oil/air stream flowed through openings in the outer bearing spacer and impinged on the ball bearings. It then passed through the bearings and out two ports on the lower upstream and downstream ends of the bearing sleeve. This was an open system. The used oil vented to waste buckets and was not recirculated.

3. Temperature Monitoring System

Because inadequate cooling could lead to bearing degradation, temperature-sensing thermocouples were placed in holes through the bearing housing at each bearing outer race. These were wired to digital output meters installed in the control panel in the TTR control room and were used to constantly monitor the bearing temperature and insure that the cooling system was operating effectively. The redesigned bearing housing assembly was rebalanced successfully at approximately 2500 rpm, with the oil-mist

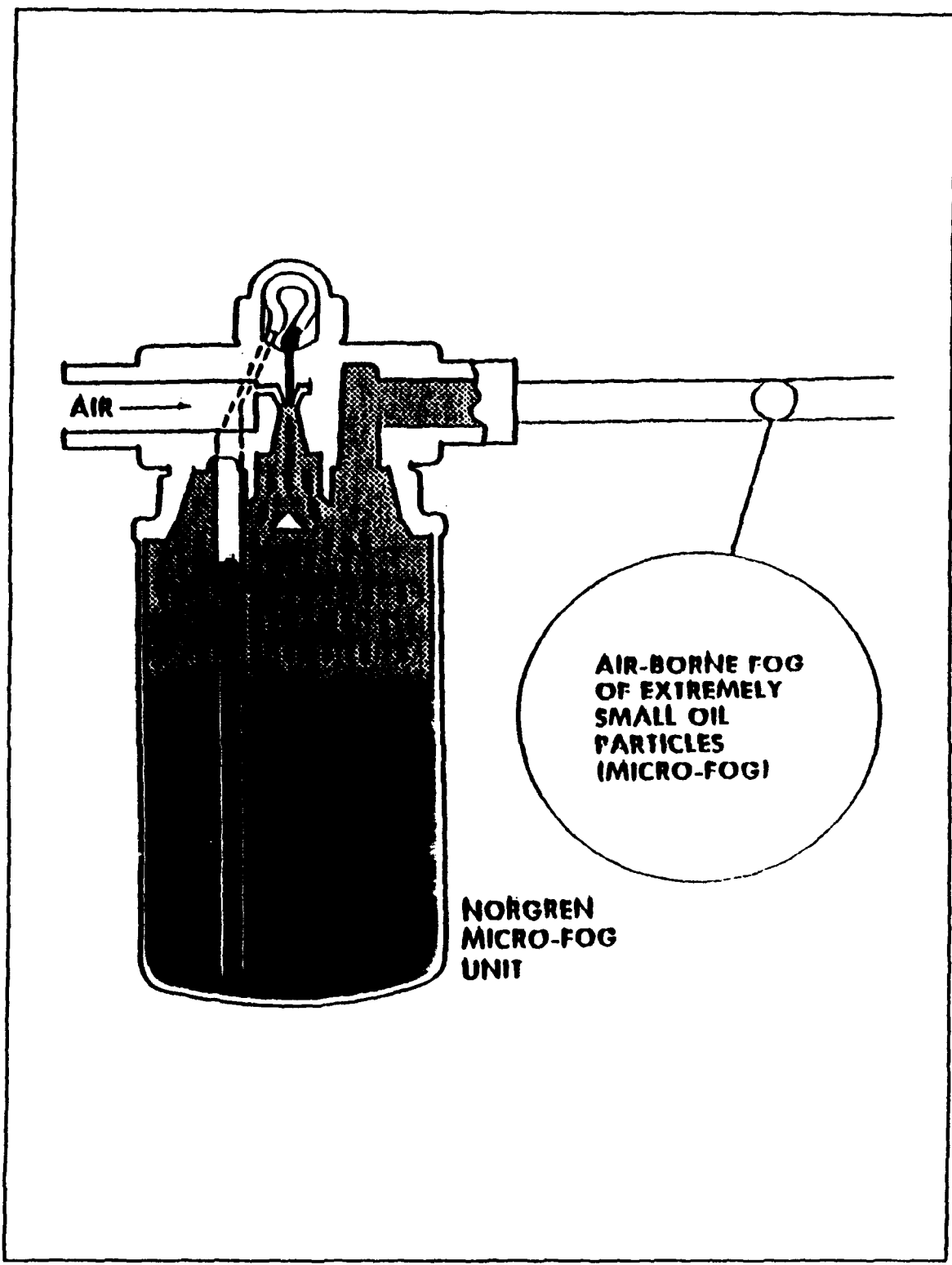


Figure 4. Oil Mist Cooling System

lubrication system operating. The temperature-monitoring system was installed, and the assembly was put into service.

4. Vibration Monitoring System

In order to ensure the safety of operating the TTR, a vibration-detection system was installed to detect possible out-of-balance conditions and bearing degradation. The vibration-sensing system consisted of four accelerometers and a signal analyzer. All four accelerometers were attached to the bearing-housing support. One was upstream at the top of the housing and the second was upstream but displaced 90° clockwise looking upstream. The remaining two accelerometers were installed on the two bearing-housing support struts. The first two were wired directly into a Scientific-Atlanta SD380 Signal Analyzer in the control room. The two accelerometers installed on the support struts were wired into the control panel, and to an analog Ballantine Laboratories RMS indicator. From the analog indicator, they could be connected (if needed) to the signal analyzer for digital processing and hard copy output.

Prior to powering the turbine with air flow, it was analyzed to determine natural frequencies so that resonance at those frequencies could be avoided. The accelerometers were installed and wired to the signal analyzer before any of the inlet ducting was attached. The stationary turbine and bearing housing assembly was struck with a modally tuned

hammer and the response of the accelerometers was recorded by the signal analyzer. An example from the top accelerometer may be seen in Figure 5. The top trace shows the real time response and the bottom shows the frequency spectrum with the first predominant mode at 67.5 Hz. The assembly was then turned by electric motor and a belt drive at varying speeds up to 960 rpm and the largest amplitude responses were found and graphed, as shown in Figure 6. Trace A is from the top accelerometer and shows the 16 Hz speed signal along with its higher harmonics. Trace B is from the accelerometer at 90°, and shows similar characteristics.

5. Control System

The control system in the TTR control room included a Fisher-Porter electronic set-point controller for the outlet valve of the hydraulic dynamometer. This was used as a speed regulator with manual or automatic modes and was unchanged from the configuration described by Studevan [Ref. 1] and Kane [Ref. 6]. In the automatic mode, the controller received a conditioned feedback signal from a magnetic speed sensor in the dynamometer. The controller compared the speed signal to a set-point and produced a corrective signal. The corrective signal, received by the outlet valve, controlled the water level in the dynamometer. The speed varied in response to the resistance produced by the

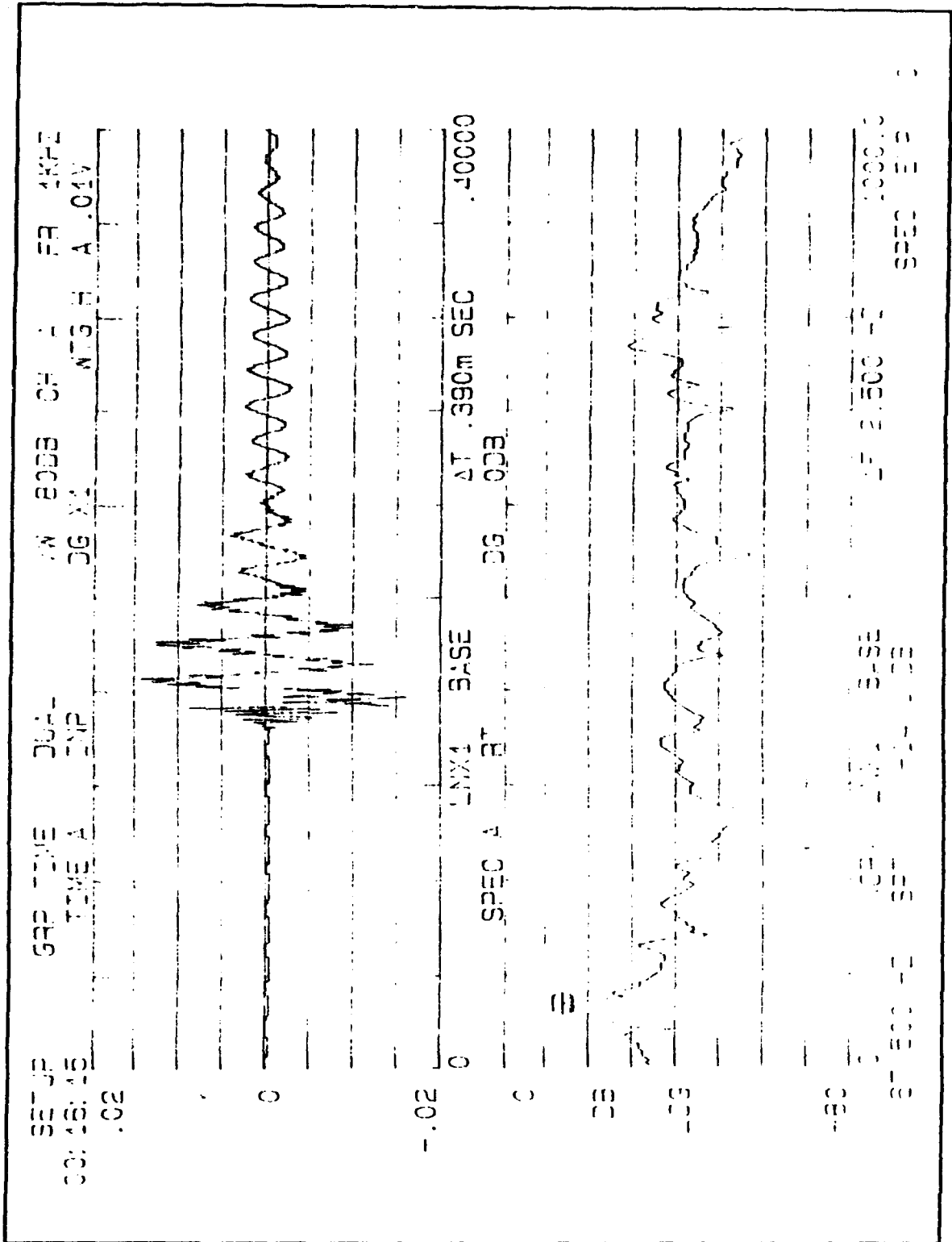


Figure 5. Stationary Shaft Impact Response

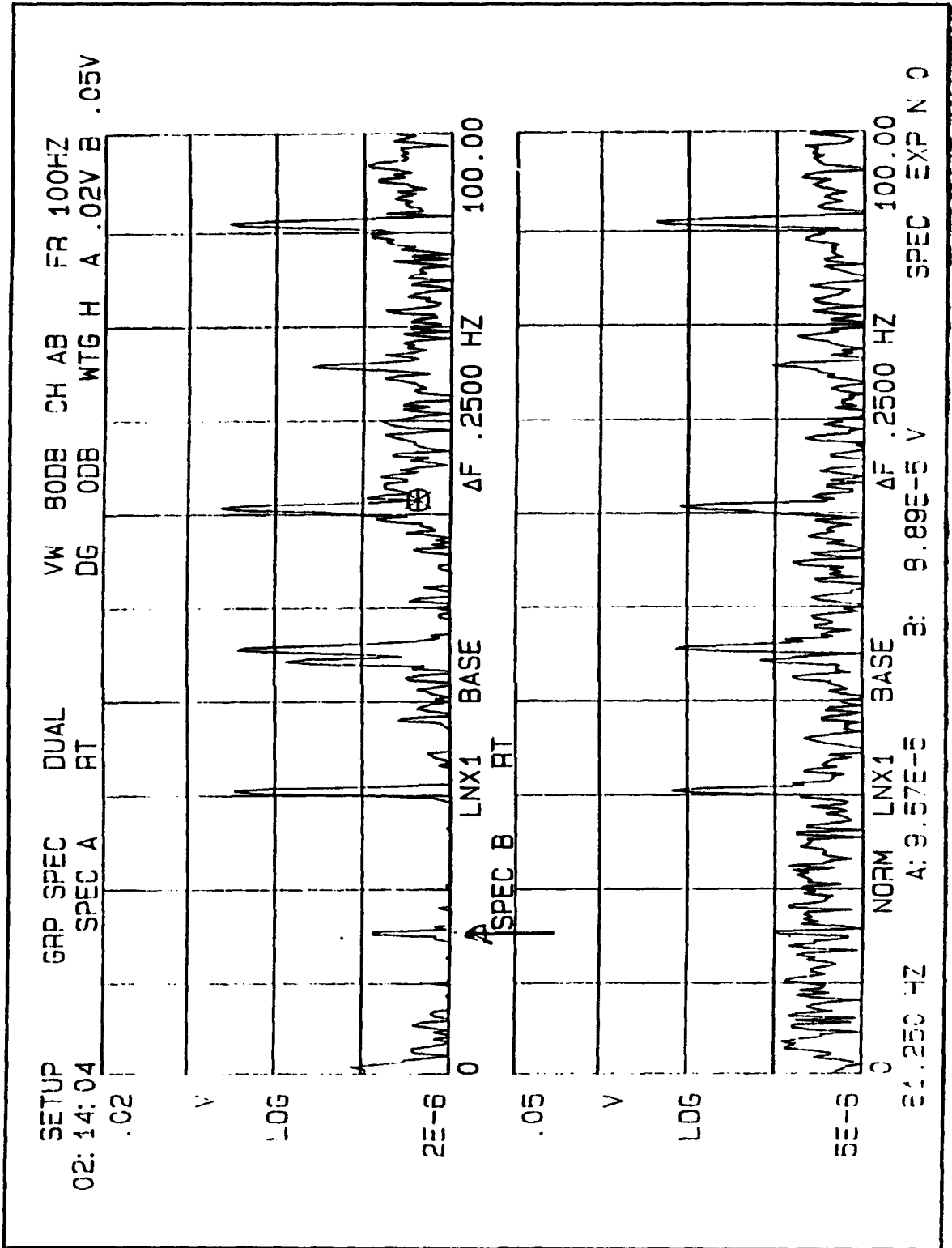


Figure 6. Motor Actuated Rotational Vibration Response

water and the energy was dissipated into the water as heat. The manual inlet control valve was also located in the TTR control room. Manual operation of the speed control system was used during all the tests conducted in the present study.

6. Probe Placement

A probe access hole was cut through the outer casing of the turbine upstream of the first-stage stator. The hole location corresponded with the inlet of the grid designed to be used in the computer simulation of the flow field. A probe holder was designed and manufactured to hold the probe in place on the test rig. It was designed to be used in any position around the circumference of the turbine. However, a new access hole would need to be cut in order to use it in another position. An engineering drawing of the probe holder may be found in Appendix A.

Combination probes (numbers 2 and 3) were placed in the inlet duct through holes cut in the piping. They were positioned at the same axial station to measure stagnation temperature and stagnation pressure into the turbine. Combination probe number 4 was clamped to the table immediately downstream of the turbine to measure exit stagnation temperature and pressure.

III. EXPERIMENT

A. EXPERIMENTAL PROCEDURE

Before any measurements were attempted in the TTR, the shroud inserts between the blade tips and the turbine outer casing were removed. With the shroud inserts removed, there was no danger of blade tips rubbing due to misalignment. Initial system validation runs documented herein were conducted with the shroud inserts removed. The TTR was operated twice to gain experience, test safe operating methods and 'shake-down' the facility. During the first shake-down run, speed control and vibration response were tested under various air and water flow settings. It was noted that if water flow was sufficiently reduced by closing the outlet valve to the dynamometer, the speed of the turbine climbed rapidly. On inspection of the TTR after the run, the dynamometer was found to be very hot. During inspection of the water-circulation system, water was found to have overflowed onto the floor of the pumping station due to surging developed by changing demand to the dynamometer. It was decided that the water flow through the dynamometer should be set at the start of the run to keep the dynamometer cool and eliminate surging of the water circulation system.

For the second shake-down run, a specific procedure was adopted to set the water and air flow at the start of the run. In order to keep sufficient and consistent water flow through the dynamometer, the inlet valve to the dynamometer was set to 80% open and the outlet valve was set to 50% open. For mass flow to the TTR to be properly calculated, all the air flowing through the metering orifice had to go to the turbine (Fig. 7). To ensure that all air flow went to the turbine, the number-two dump valve had to be completely closed. After the TTR inlet valve was set to 20% open, the number-two dump was closed, then the number-one dump valve was set to 40% open. Further manipulation of the mass flow to change the speed of the turbine involved opening the TTR inlet valve to increase speed or opening the number-one dump to decrease speed. It was necessary to have some air venting through dump valve number one in order to keep the total flow rate sufficiently high or the Allis-Chalmers compressor (Fig. 7) could surge due to excessive back pressure.

During the experimental run, the procedure described above for setting water and air flow was followed. Pauses were made during the acceleration and system settings were noted. At each pause, the speed was allowed to stabilize and measurements were made of temperatures and pressures for the power output and mass flow calculations. Measurements relevant to power calculations are shown in Table I.

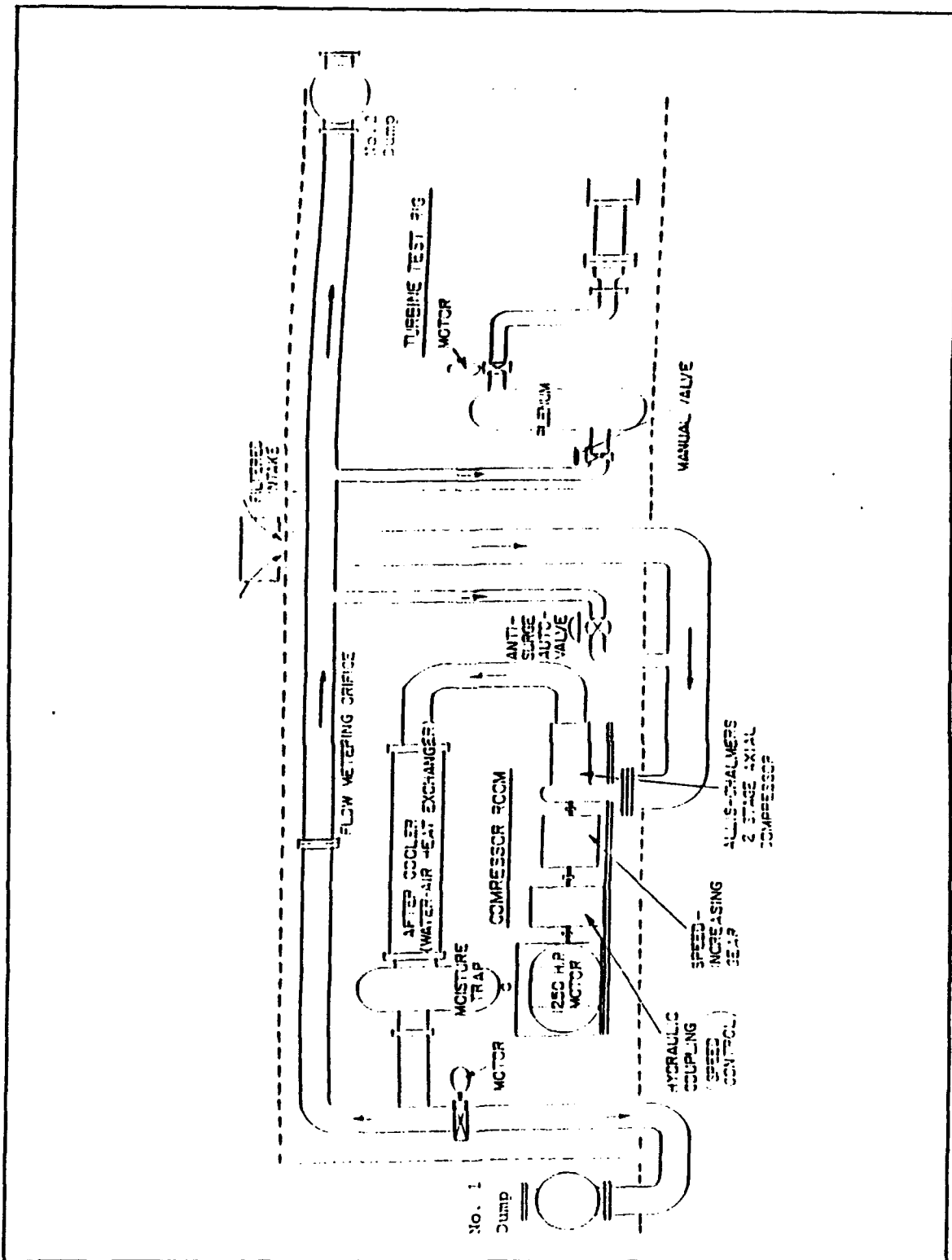


Figure 7. Compressed Air System

TABLE I. ABBREVIATED TTR DATA

Speed (RPM)	t_1 (°F)	h_w (in.H ₂ O)	P_1 (in. Hg)	TT4 (°F)	TT3 (°F)
880	81	0	37.35	77	81
1420	88	18.438	38.57	84	88
1560	92	19.000	38.98	86	92
2100	94	16.625	41.42	87	94
3700	97	24.500	53.23	84	97
5950	105	33.750	49.56	76	105
7900	111	17.375	55.06	71	111

B. MASS FLOW AND POWER CALCULATIONS

The turbine air mass-flow rate was metered by an orifice plate (Fig. 7) and was calculated using the method described by Vavra [Ref. 16] and summarized in Appendix B. The power output of the turbine was calculated using the stagnation temperature drop of the air across the turbine, and the mass flow rate. Table II shows calculated values of mass-flow rate, specific power out of the turbine, and efficiency. Details of these calculations may be found in Appendix C and a complete table of measurements is contained in Appendix D.

TABLE II. TURBINE PERFORMANCE (SHROUDS REMOVED)

Speed (RPM)	Mass Flow Rate (lbm/s)	Specific Power (Hp/lbm)	Efficiency (%)
880	-	-	14.96
1420	7.51	1.35	7.47
1560	7.63	2.03	9.98
2100	7.37	2.36	6.48
3700	10.08	4.40	3.86
5950	11.27	9.81	3.49
7900	8.57	13.53	3.23

IV. NUMERICAL SIMULATION

A. GRID GENERATION

Numerical simulation of a flow field is highly dependent on the grid used to define the geometry, and its resolution. Many routines have been developed to generate grids within and about realistic surfaces that bound fluid flows. The computer program used to develop the grids used in this investigation, Turbomachinery C-Grid (TCGRID), generates three-dimensional C- or H-type volume grids for turbomachinery. Grid files are compatible with RVC3D and PLOT3D [Ref. 7] which were used extensively in the flow solution and visualization.

TCGRID generates a three-dimensional computational volume grid in the following manner:

1. A coarse, equally-spaced meridional grid is generated between the supplied hub and tip.
2. The blade geometry is interpolated onto the meridional grid.
3. 2-D blade-to-blade grids are generated along the meridional grid lines in $(m, rbar*theta)$ coordinates using an old version of the Sorenson GRAPE code [Ref. 8].
4. The $(m, rbar*theta)$ coordinates are transformed to $(z, r, theta)$ coordinates.
5. The 2-D grids are reclustered spanwise to make a full 3-D grid.

6. Finally, the (z,r,theta) coordinates are transformed back to (x,y,z) and written in PLOT3D format.

Hub, tip and blade geometries must be in MERIDL [Ref. 9] format.

The hot-flow blade geometry data were received from NASA Lewis Research Center [Ref. 10] in (z,r,theta) coordinates appropriate for use in TCGRID. Since the Naval Postgraduate School facility was cold-flow, a 99% thermal-shrink factor had to be applied to all linear dimensions. The FORTRAN code written to accomplish this may be seen in Appendix D.

Grid generation and sizing is a subjective exercise in which there is no single 'right' answer. Often the success of a grid remains unknown until it is used with a flow solver. In this investigation, over one hundred flow solutions were attempted with various grid sizes before a successful combination was found. It was understood that the investigation required a fully three-dimensional viscous flow solution. Because of the resolution needed in the boundary layer, the grid had to be very fine. However, the successful grid contained more than twice the number of grid points in the spanwise direction than originally thought. The final grid size used for the flow solutions was 151 x 31 x 45. Chima [Ref. 11] recommended 15 grid points in each endwall boundary layer for good resolution. An example of the TCGRID input file may be found in Appendix D.

Figures 8 through 11 show C-grids developed by TCGRID for the hub, midspan and tip.

This geometry was difficult to model because of the endwall contour (Fig. 8). The hub and tip geometry was defined in the input file with (z,r) coordinates. Then the stator contour was defined in five sets of (z,θ,r) coordinates. Each set of coordinates was at a constant radius. Since the endwall radius reduced at the stator tip, some of the coordinates were defined outside the endwall. TCGRID calculates the intersection of the stator coordinates with the endwall and generates the grid defined by the intersection contour. Figures 9 through 11 show grids developed for hub, mean and tip sections. Figure 12 shows a three-dimensional view of the final grid. The curved trailing edge shown in this figure also complicated the grid generation procedure.

B. FLOW SOLUTION

1. RVC3D

Once a proposed grid has been developed, it can be used by a flow solver to simulate a flow. RVC3D (Rotor Viscous Code 3-D) is a computer code developed at NASA Lewis Research Center for the analysis of fully three-dimensional viscous flows in turbomachinery. The code solves the thin-layer Navier-Stokes equations with an explicit finite-difference technique. It is applicable to annular blade

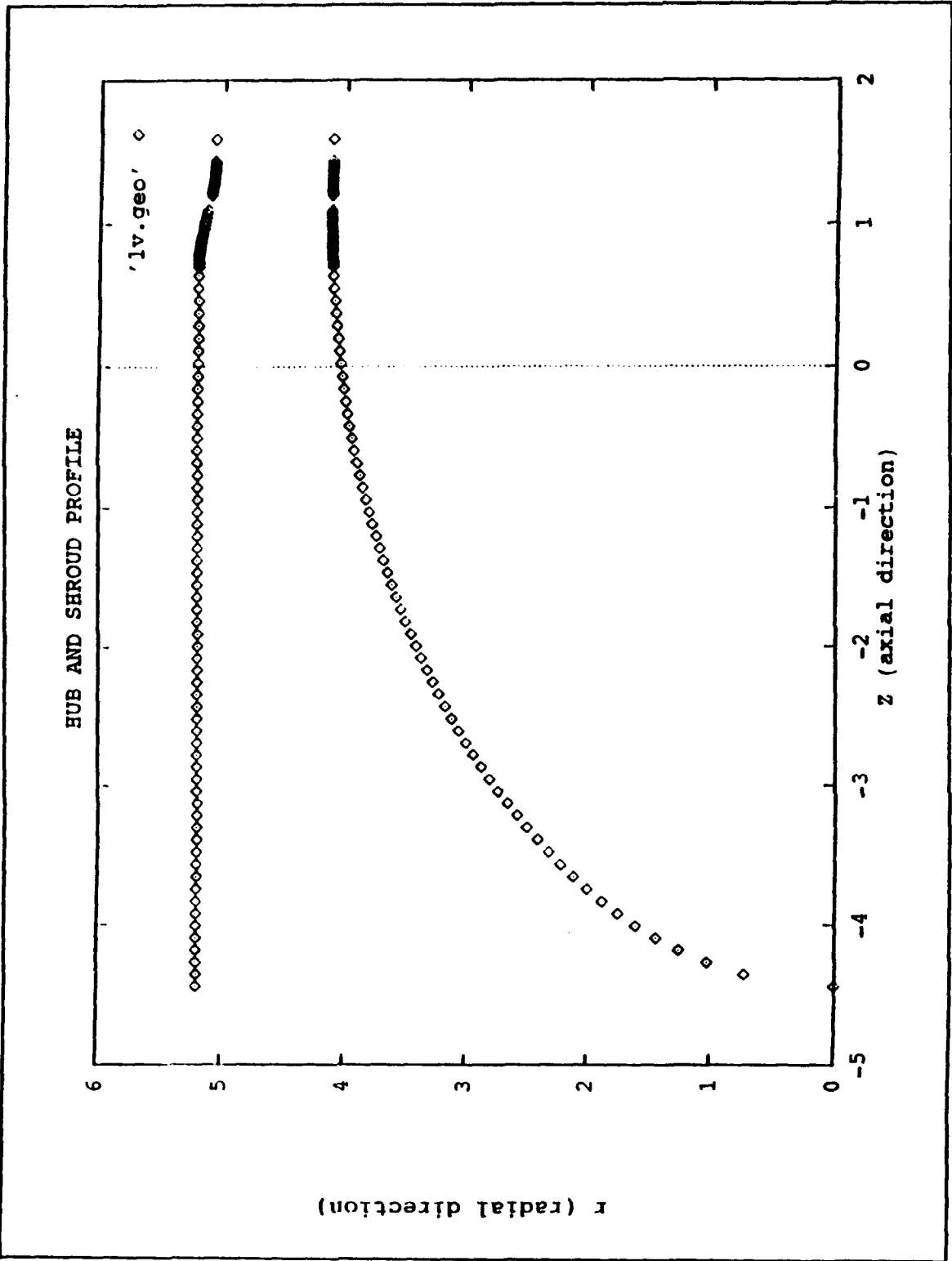


Figure 8. Hub and Endwall Contour

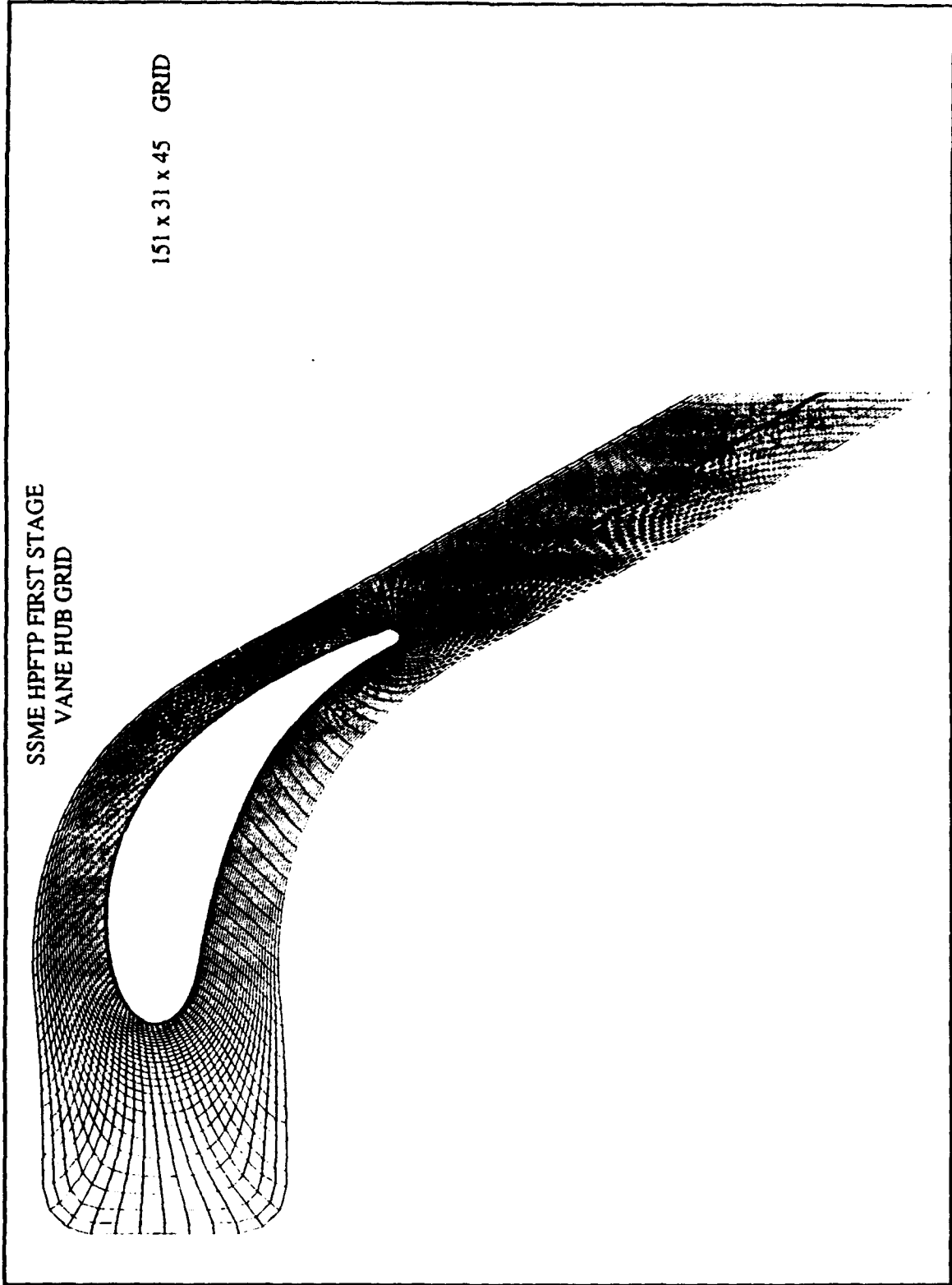


Figure 9. C-Grid at Stator Hub

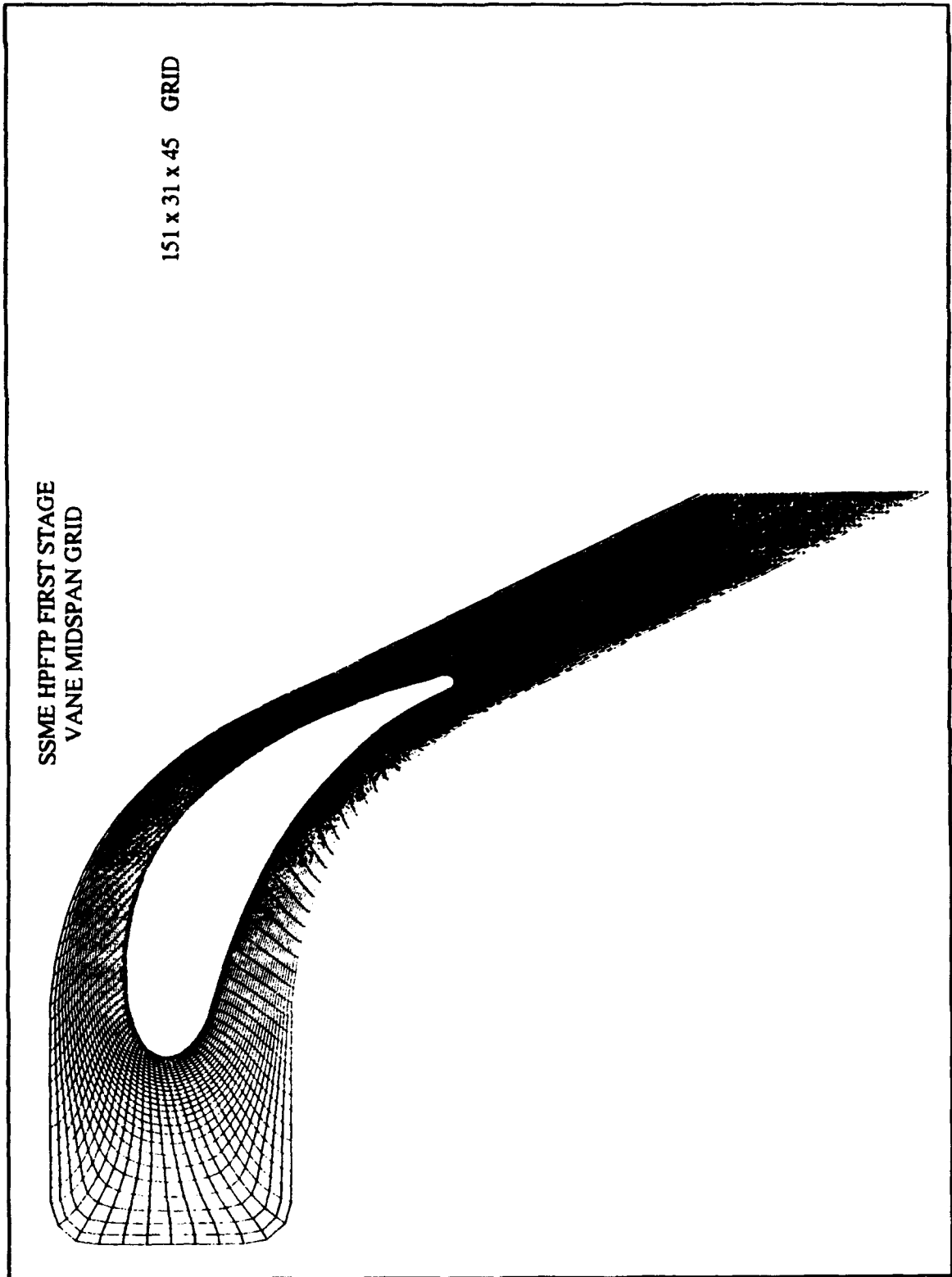


Figure 10. C-Grid at Stator Midspan

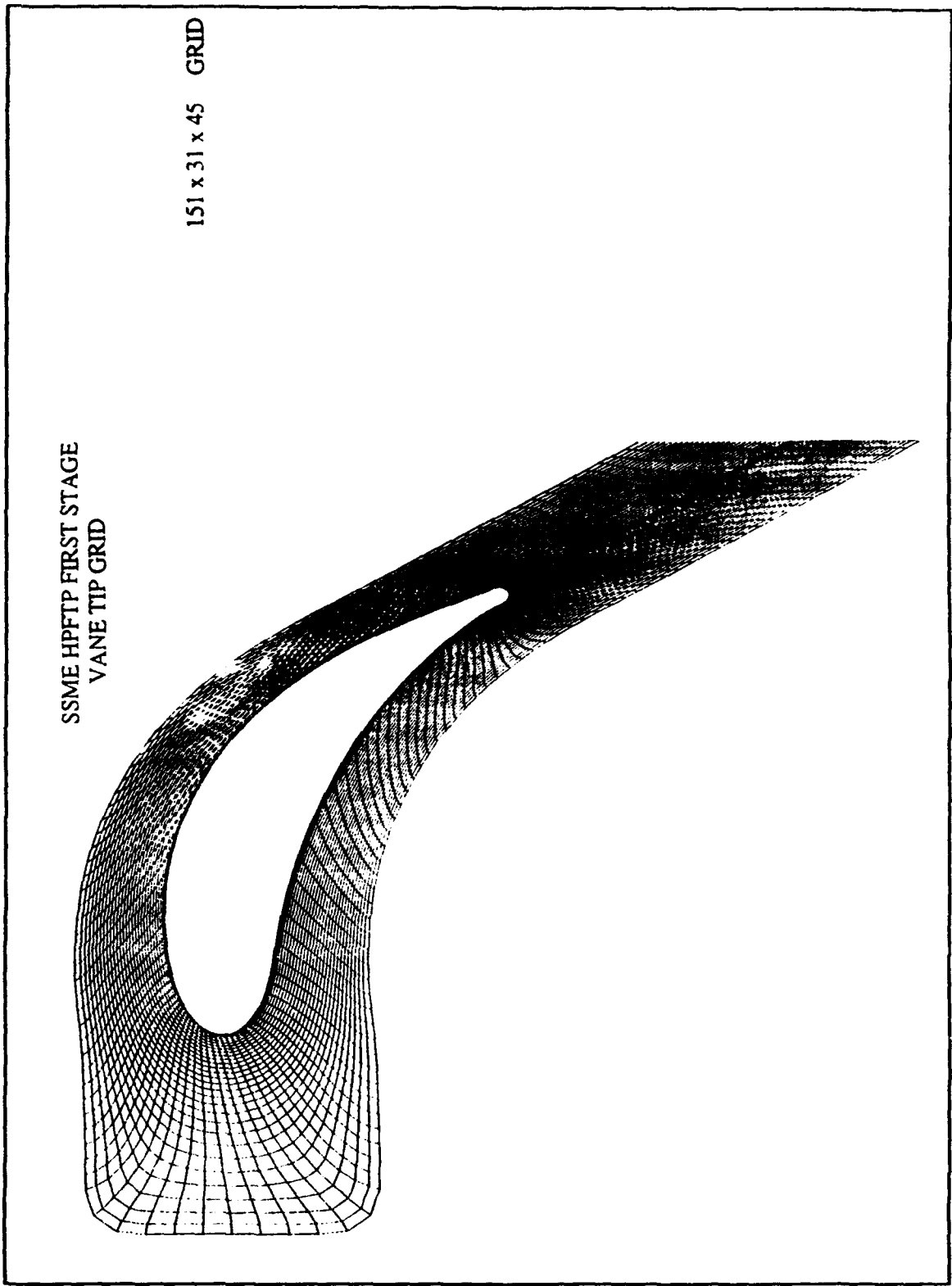


Figure 11. C-Grid at Stator Tip

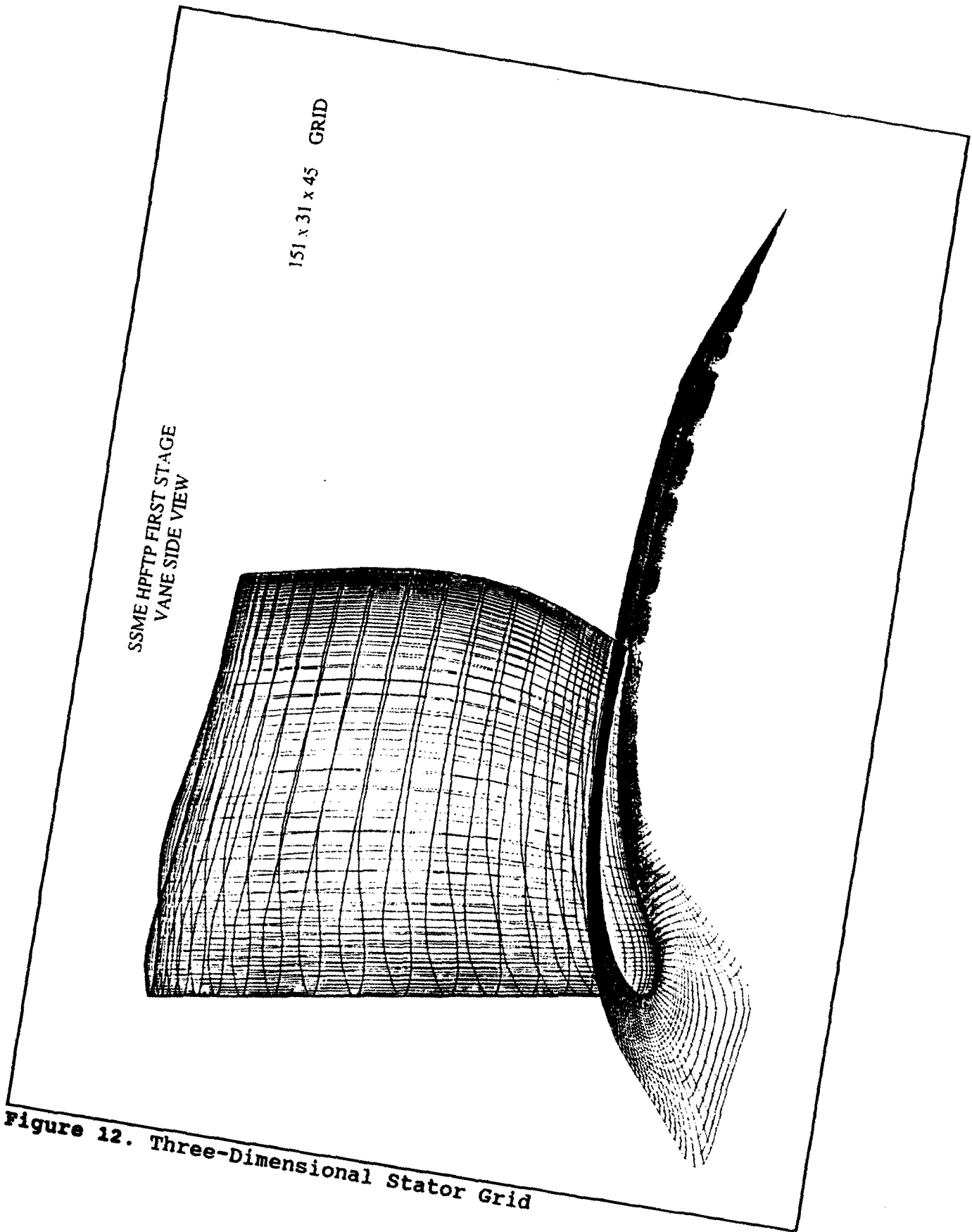


Figure 12. Three-Dimensional Stator Grid

rows or linear cascades and includes two turbulence models along with a simple tip clearance model. Mathematical formulation of RVC3D is described in references 12 and 13.

The code solves the Navier-Stokes equations in Cartesian coordinates with rotation about the x-axis. The equations are mapped to a general body-fitted coordinate system (Fig. 13). Turbulence is modelled using a three-dimensional adaptation of the Baldwin-Lomax model [Ref. 14] or the Cebeci-Smith model [Ref. 15]. A sample RVC3D input file may be seen in Appendix D.

2. Solution Method

Simulations were run on two different computer systems; a Silicon Graphics Iris workstation and a Cray Y-MP EL-98 supercomputer. Both systems reside at the Naval Postgraduate School. Solutions were obtained for two inlet velocity profiles on each machine. The same version of RVC3D was loaded onto the two computers and identical input files were used.

First, using the two computers for time efficiency, an inlet velocity profile to simulate a fully developed turbulent flow was found using the Iris while, concurrently, a profile simulating a slug flow inviscid profile was found using the Cray. The profiles were developed by modifying the RVC3D input files and running 100 iterations at a time to find the inlet velocity profile. After each run, the

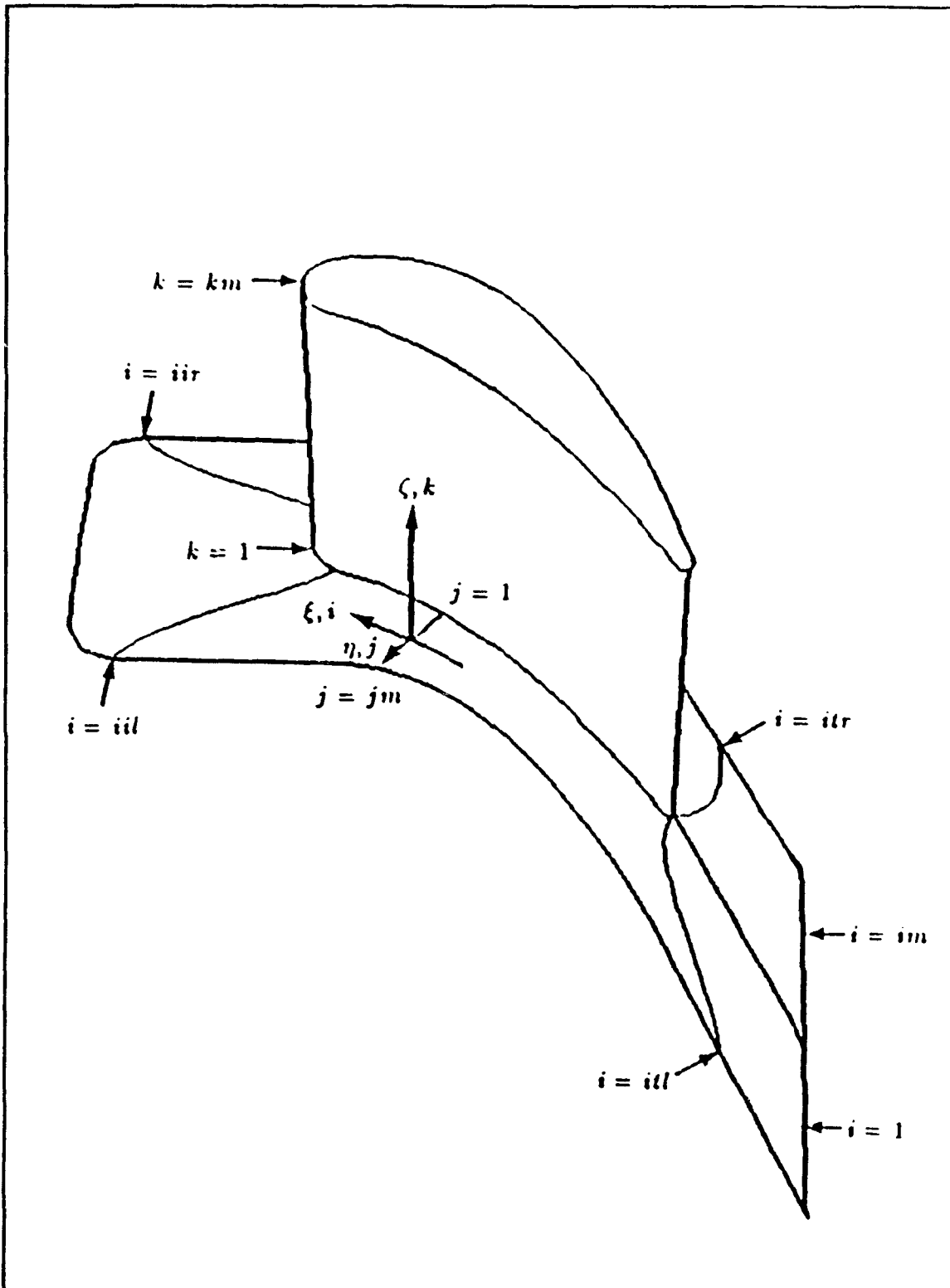


Figure 13. General Body-Fitted Coordinate System

input file was modified and run again. The process was repeated until a satisfactory profile was obtained. It was assumed that the two computers would yield identical results.

After several runs on each computer, it was noted that when similar values were used in the input files for the two machines, the velocity profiles that were calculated were vastly different. The turbulent velocity profile was run on the Iris until the solution converged and the same was done on the Cray with the slug profile. Then the input files were exchanged and the simulations were run again. All four solutions were plotted for comparison.

V. RESULTS AND DISCUSSION

A. EXPERIMENT

The data shown in Appendix C yield curves shown in Figures 14 and 15. The curves confirm general trends that were expected from the experiment. The data were taken without the intention of producing a turbine map but to validate the data acquisition methodology and to check the integrity of the turbine and its subsystems. The data show that the system will work but that it is inconsistent. It was noted that the water manometers used to measure pressure drop across the metering orifice were contaminated. This explains the inconsistent values noted in Appendix C as P31, P32, P33 and P34.

The difference in the stagnation temperature readings indicate that the flow may not have been circumferentially uniform. The stagnation pressure values PT2 are obviously erroneous and the data obtained with that combination probe were not used.

The low efficiencies shown in Figure 15 were expected. Since the shroud inserts were removed for these runs, it was expected that much of the air flow would pass between the blade tips and the outer case. The air passing around the

Specific Power and Mass Flow Rate vs RPM

SSME HPFTP Turbine (ATD)

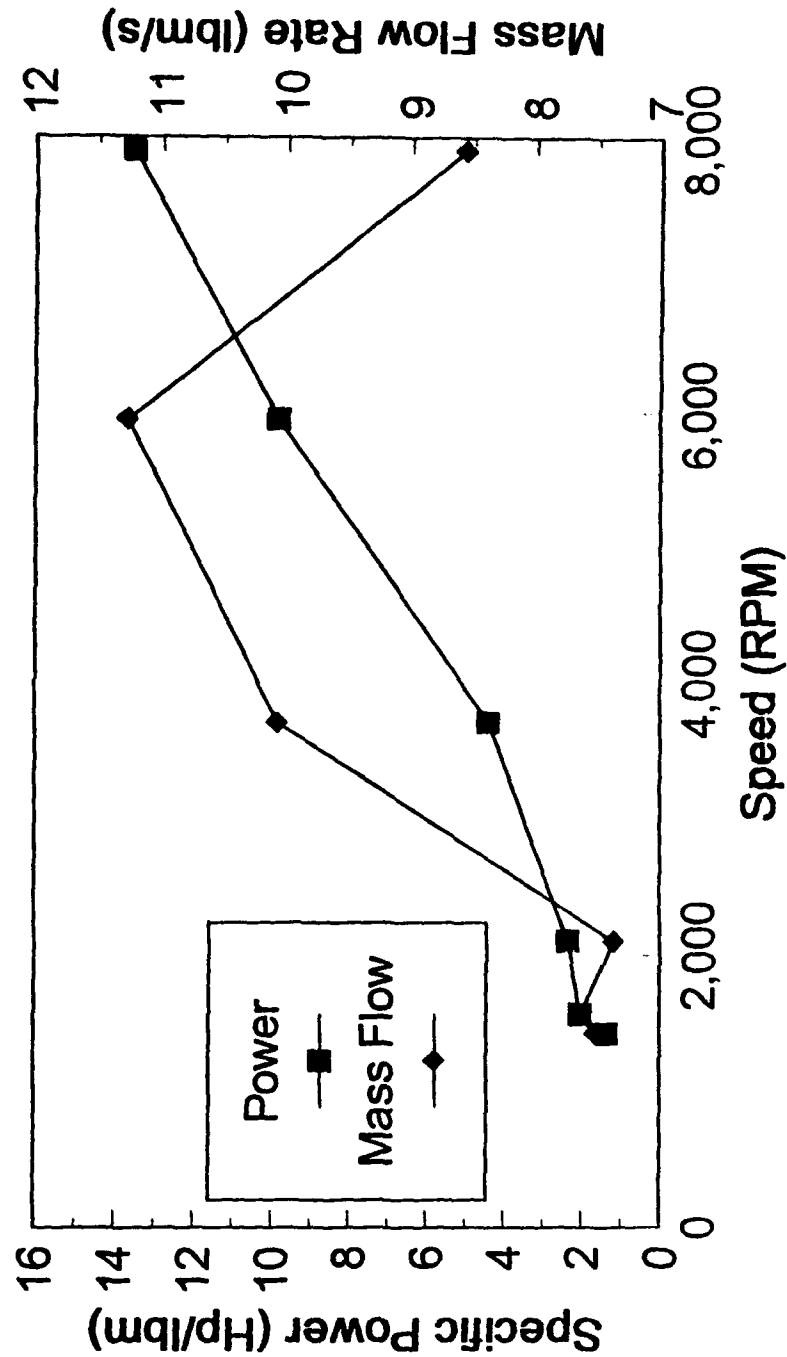


Figure 14. Specific Power and Mass Flow vs Speed

Efficiency vs RPM SSME HPFTP Turbine (ATD)

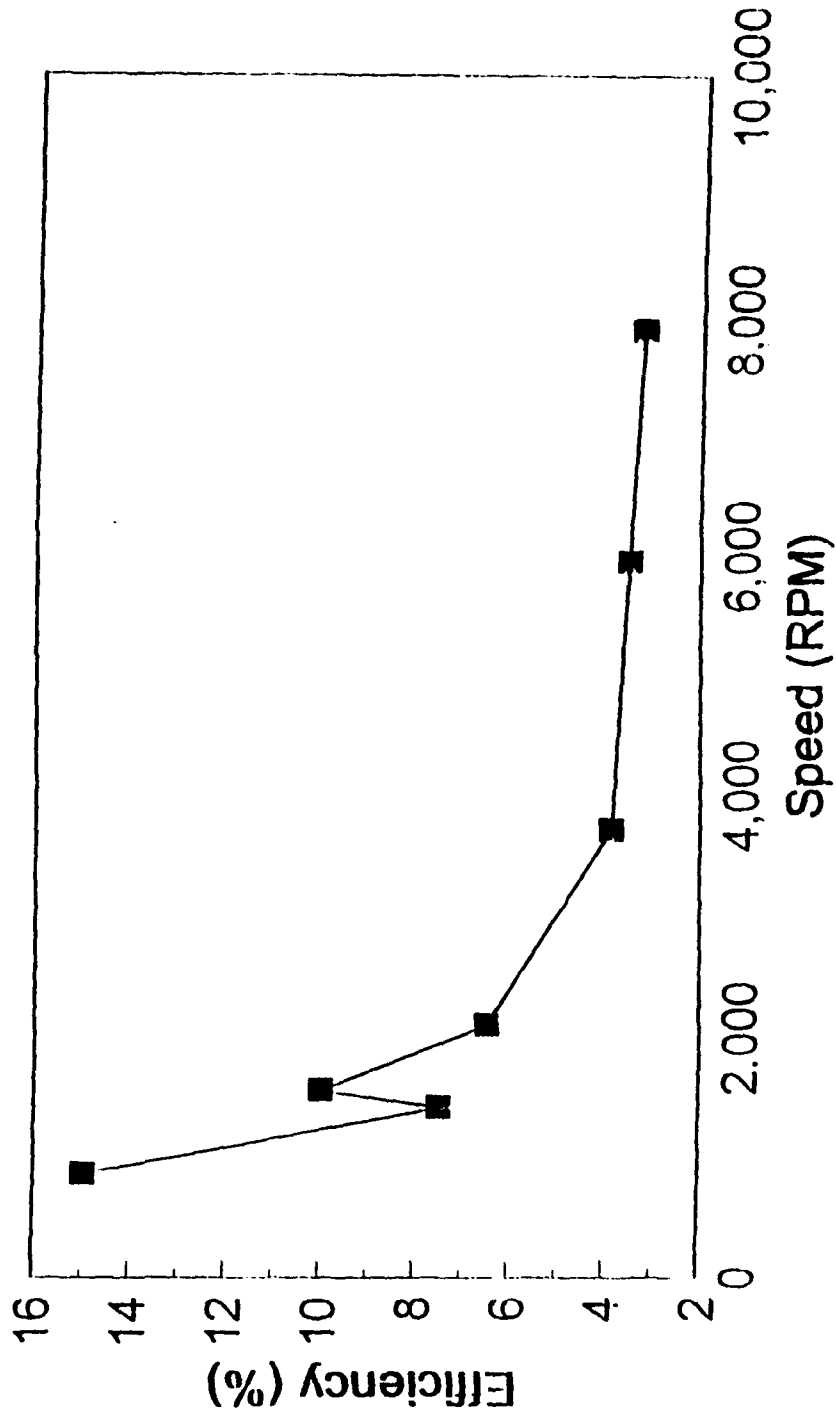


Figure 15. Efficiency vs Speed

rotor blades did not contribute to the power output of the turbine and significantly reduced the efficiency.

Figure 16 shows the speed sensor response of the TTR at 800 rpm. The number in the lower left hand corner, measured in Hertz, comes from the rotational speed. But, since the magnetic speed sensor on the dynamometer detects the passage of teeth on a 30 tooth gear, the rpm of the system is twice the frequency shown. Figure 17 shows the speed sensor response at 7925 rpm.

B. COMPUTATIONAL FLUID DYNAMICS

As noted previously, running RVC3D with the same input files on the two computers resulted in solutions with clearly different inlet velocity profiles. Figure 18 shows the two turbulent inlet velocity profiles from one input file, and Figure 19 shows the slug flow profiles from the other. The differences in inlet profiles generated in the course of the solution, show that the inlet velocity profile is sensitive to either the architecture or the precision of the particular computer.

Figures 20 and 21 show the differences in inlet velocity profiles using the two input files on the same computer. The similarity of the graphs shows that the output inlet velocity profile is not very sensitive to changes in input velocity profile. Comparison of Figures 18 and 19 with Figures 20 and 21 indicates that the output inlet velocity

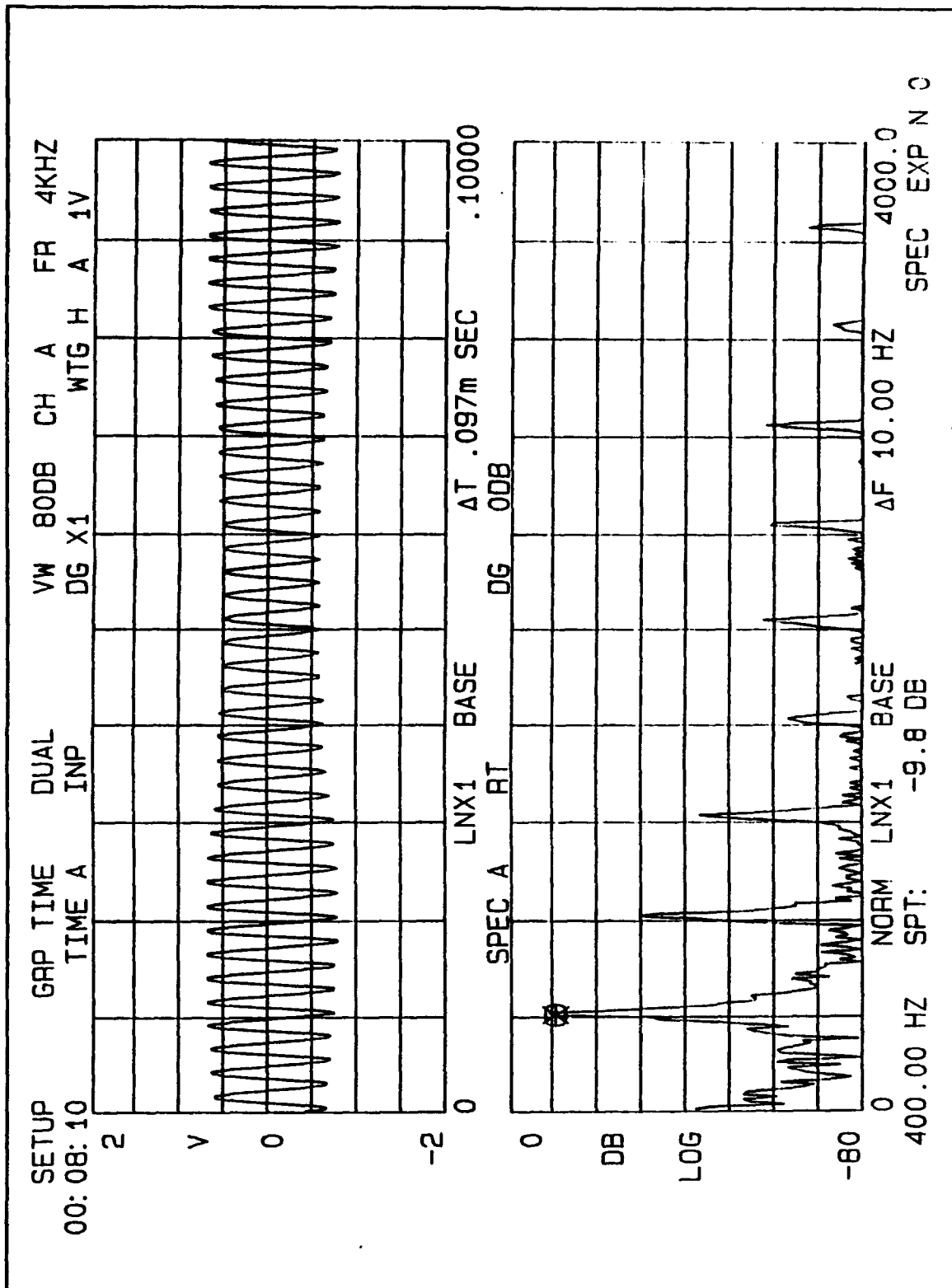


Figure 16. Low Speed Vibration Response

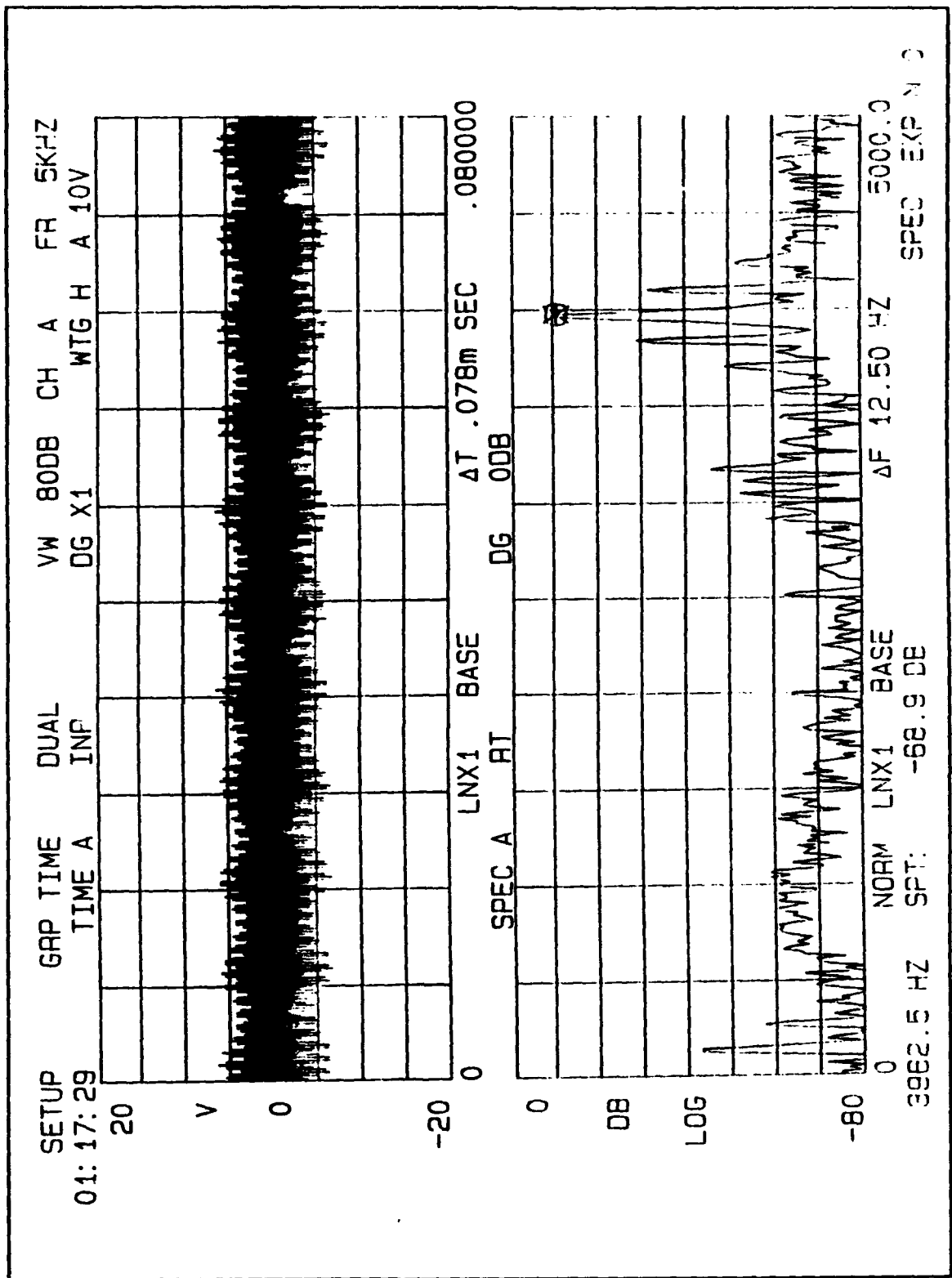


Figure 17. High Speed Vibration Response

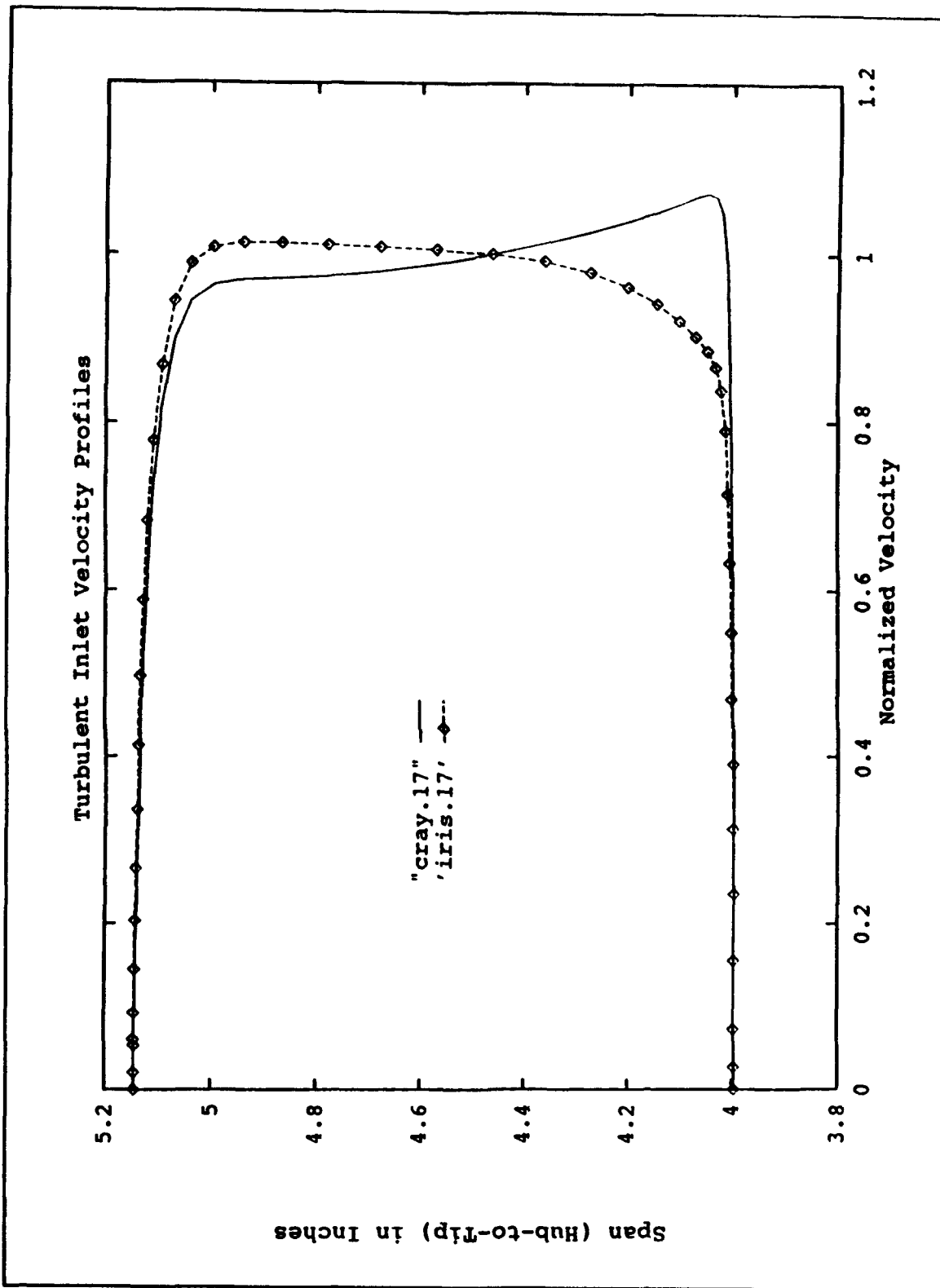


Figure 18. Turbulent Inlet Velocity Profiles

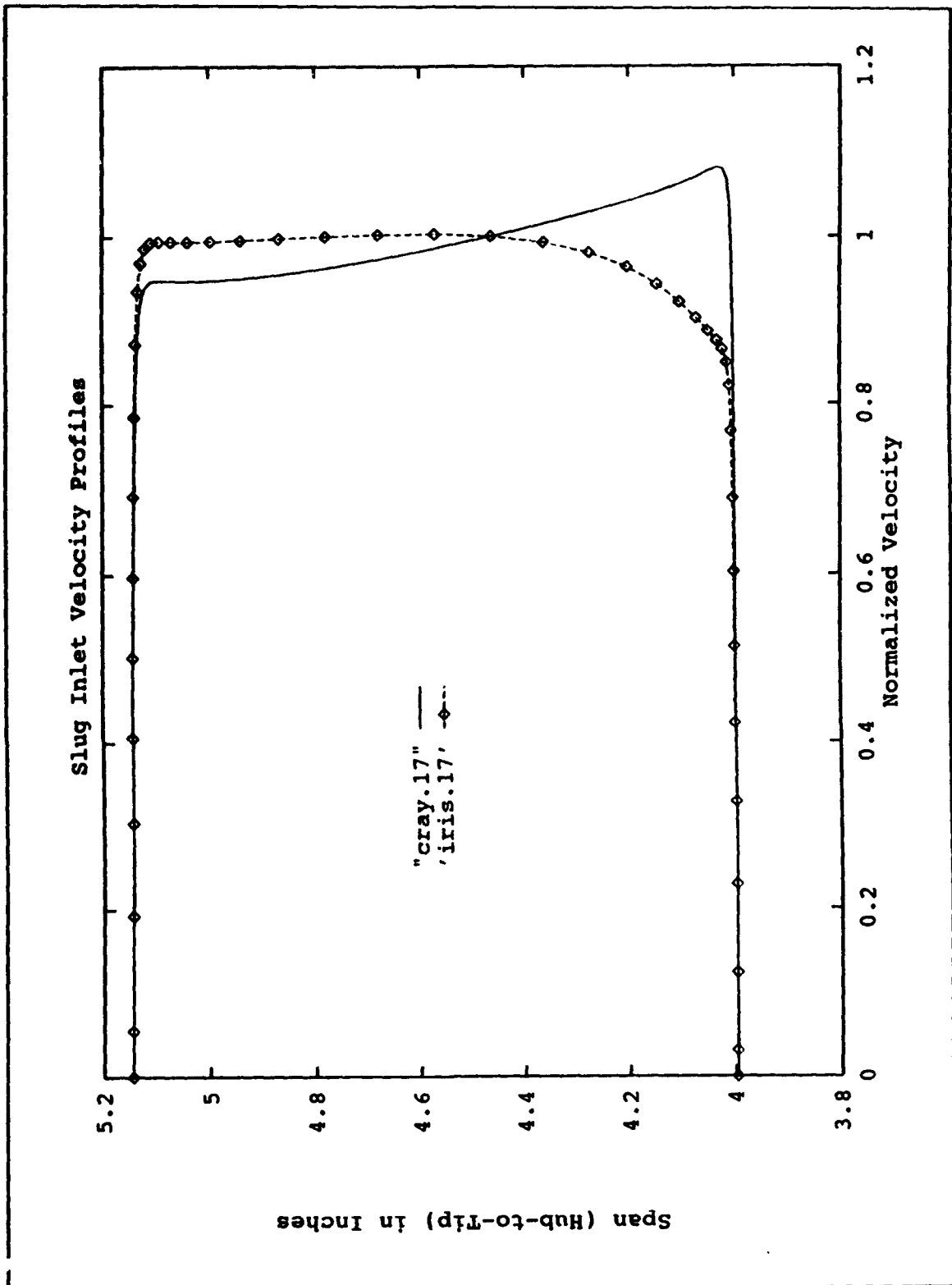


Figure 19. Slug Flow Inlet Velocity Profiles

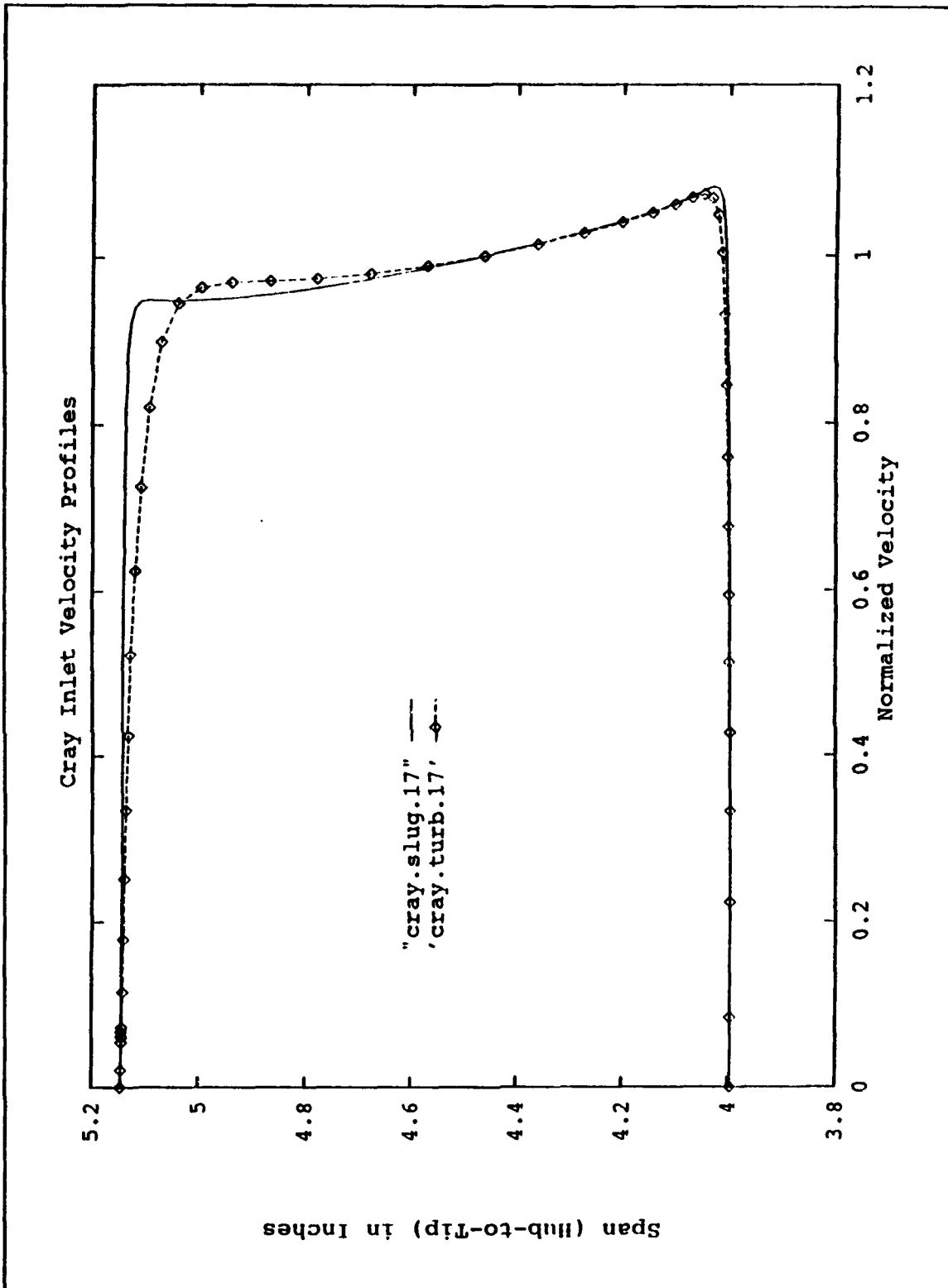


Figure 20. Cray Inlet Velocity Profiles

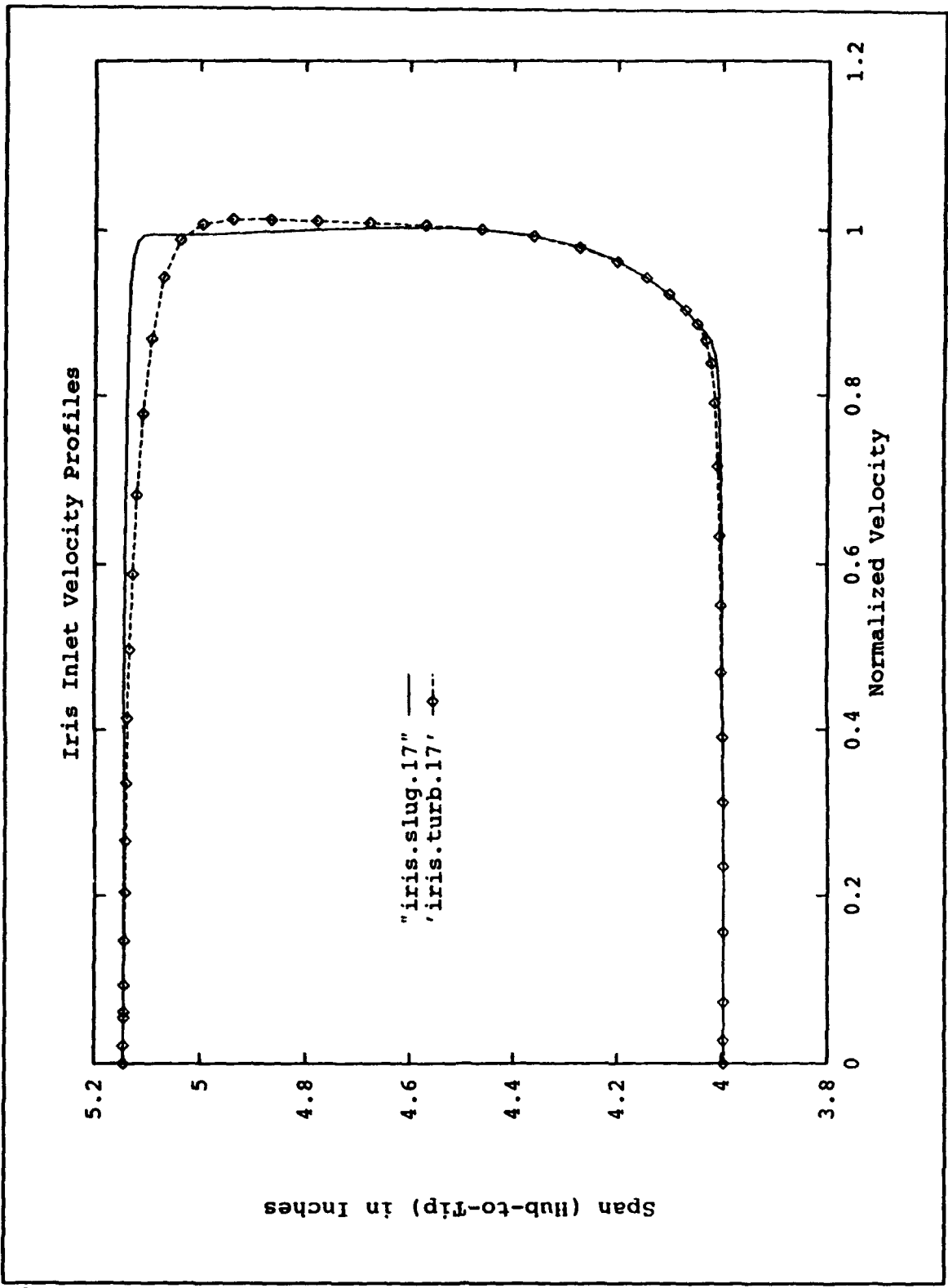


Figure 21. Iris Inlet Velocity Profiles

profile is more sensitive to computer than to input velocity profile.

Figures 22 and 23 show the midspan chordwise variation in normalized pressure distribution of solutions with the same input velocity profiles on different computers. Figures 24 and 25 show the same results with the different inlet profiles on the same machine. Comparison of these four graphs shows that all the variations gave identical pressure distributions. Therefore, the pressure distribution is sensitive to neither inlet velocity profile nor computer.

Figures 26 through 29 are PLOT3D plots of midspan Mach number contours. The first two show the Cray solutions of the turbulent and slug flow inlet velocity profiles. The latter two show Iris workstation solutions for the same input files. Again, in spite of the differences in the input files and the velocity profiles, all four solutions are identical. The plots show the flow accelerating on both the suction and pressure surfaces of the stator with maximum Mach number in the area of the throat as expected. Boundary layer growth as well as wake shape and orientation are evident in the plots.

It is important to note that the wake, in yellow, does not follow the contour of the grid but follows the exit angle of the stator. The cut that joins the pressure and suction sides of the grid may be seen in Figure 10. The

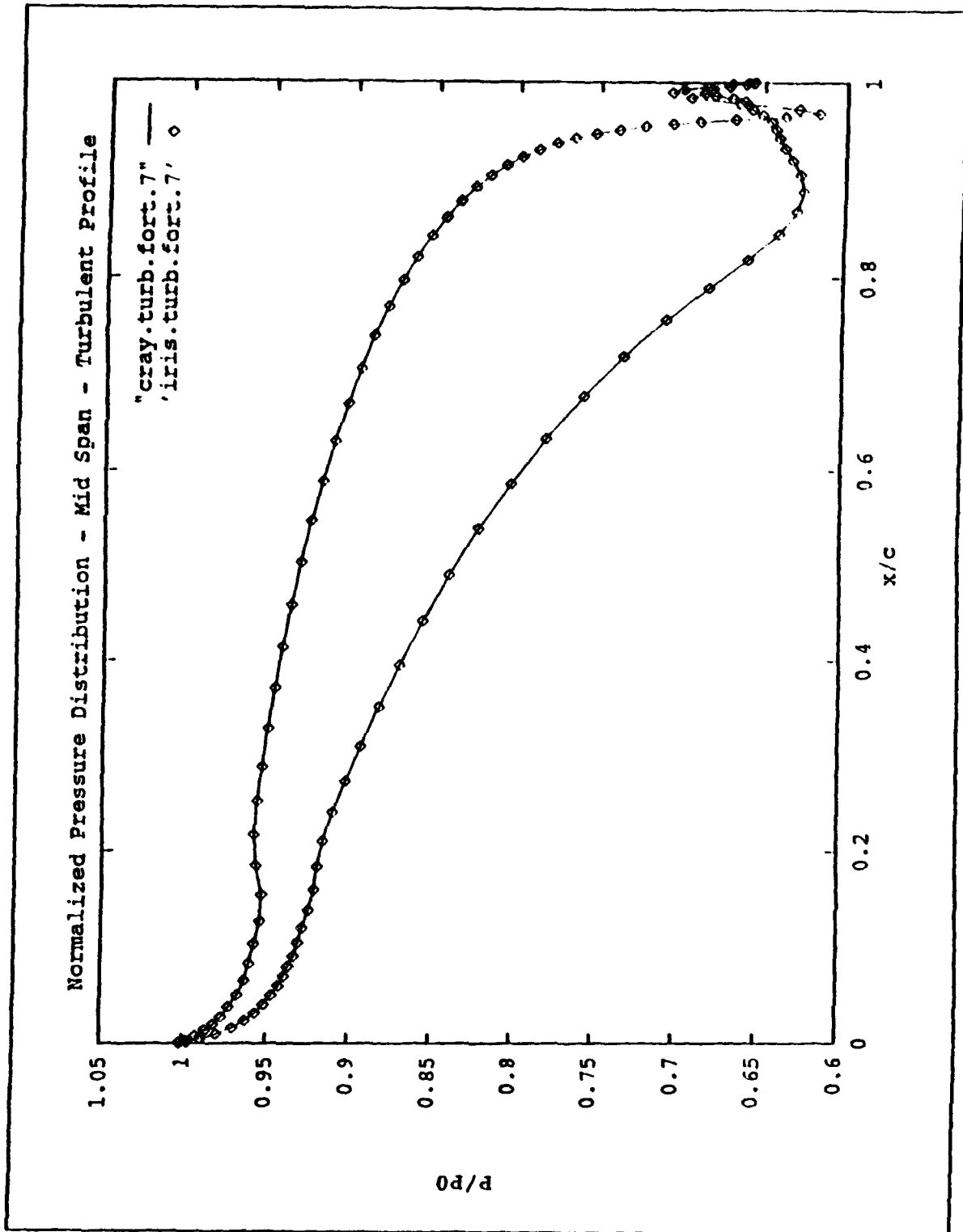


Figure 22. Normalized Pressure - Turbulent

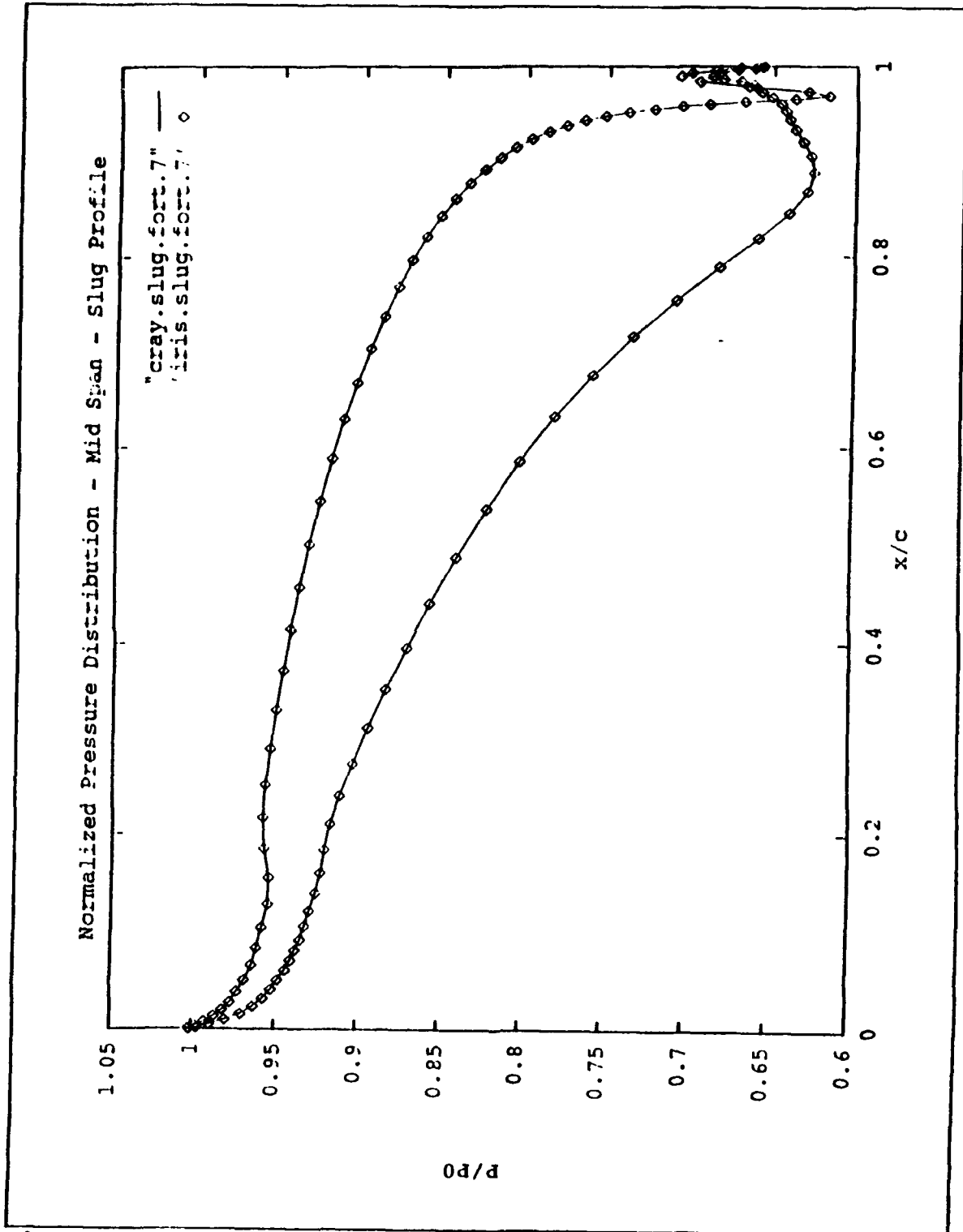


Figure 23. Normalized Pressure - Slug Flow

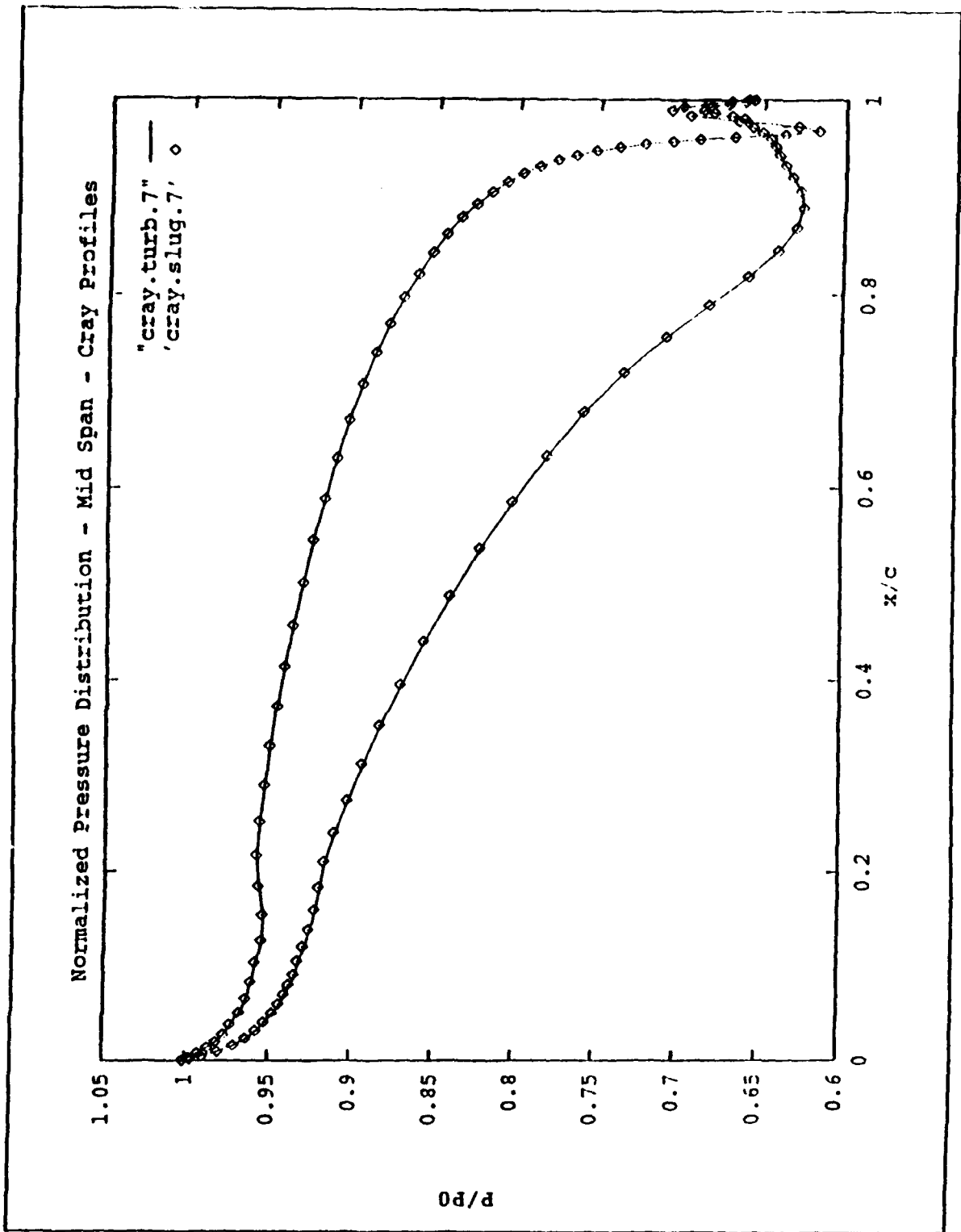


Figure 24. Normalized Pressure - Cray

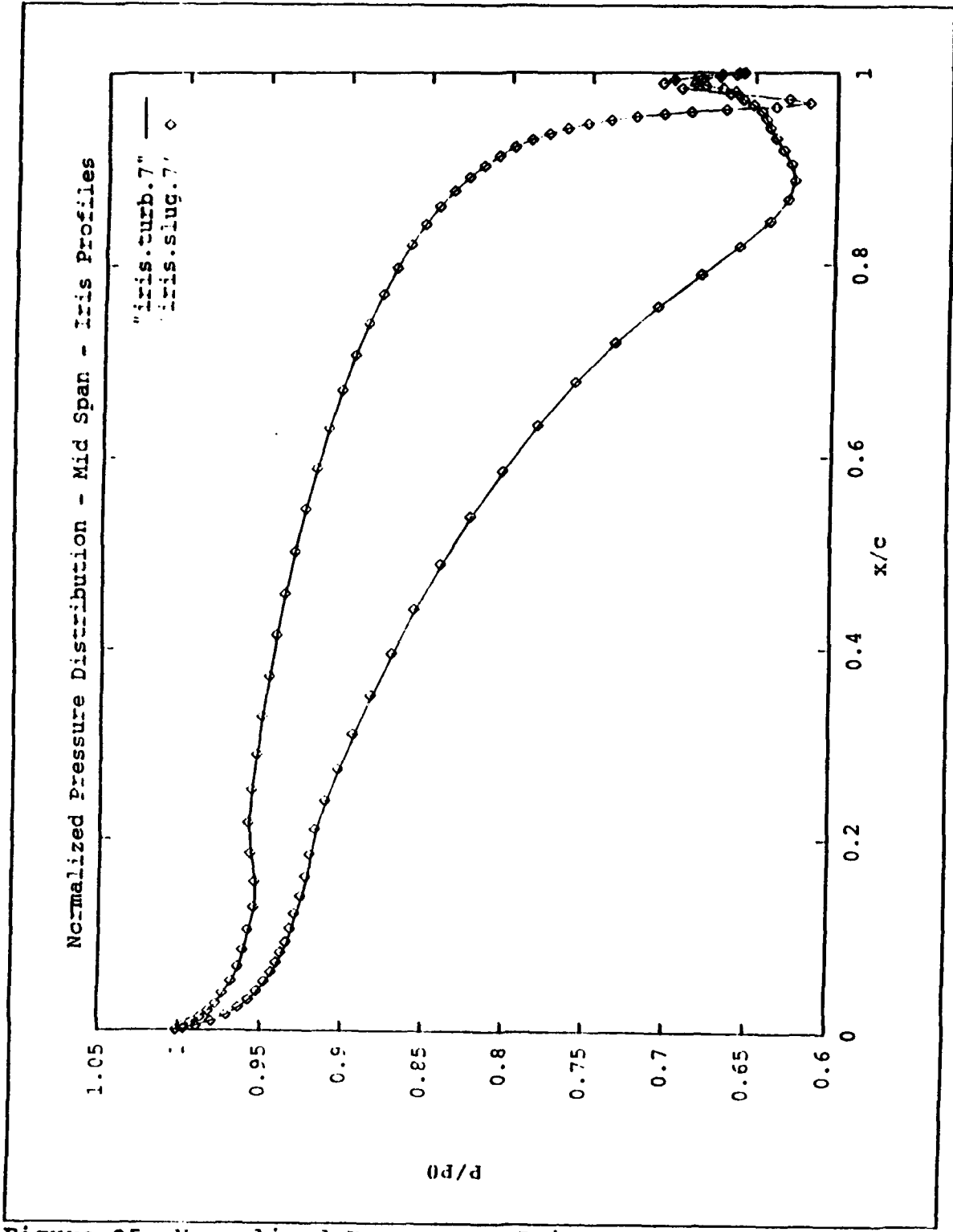


Figure 25. Normalized Pressure - Iris

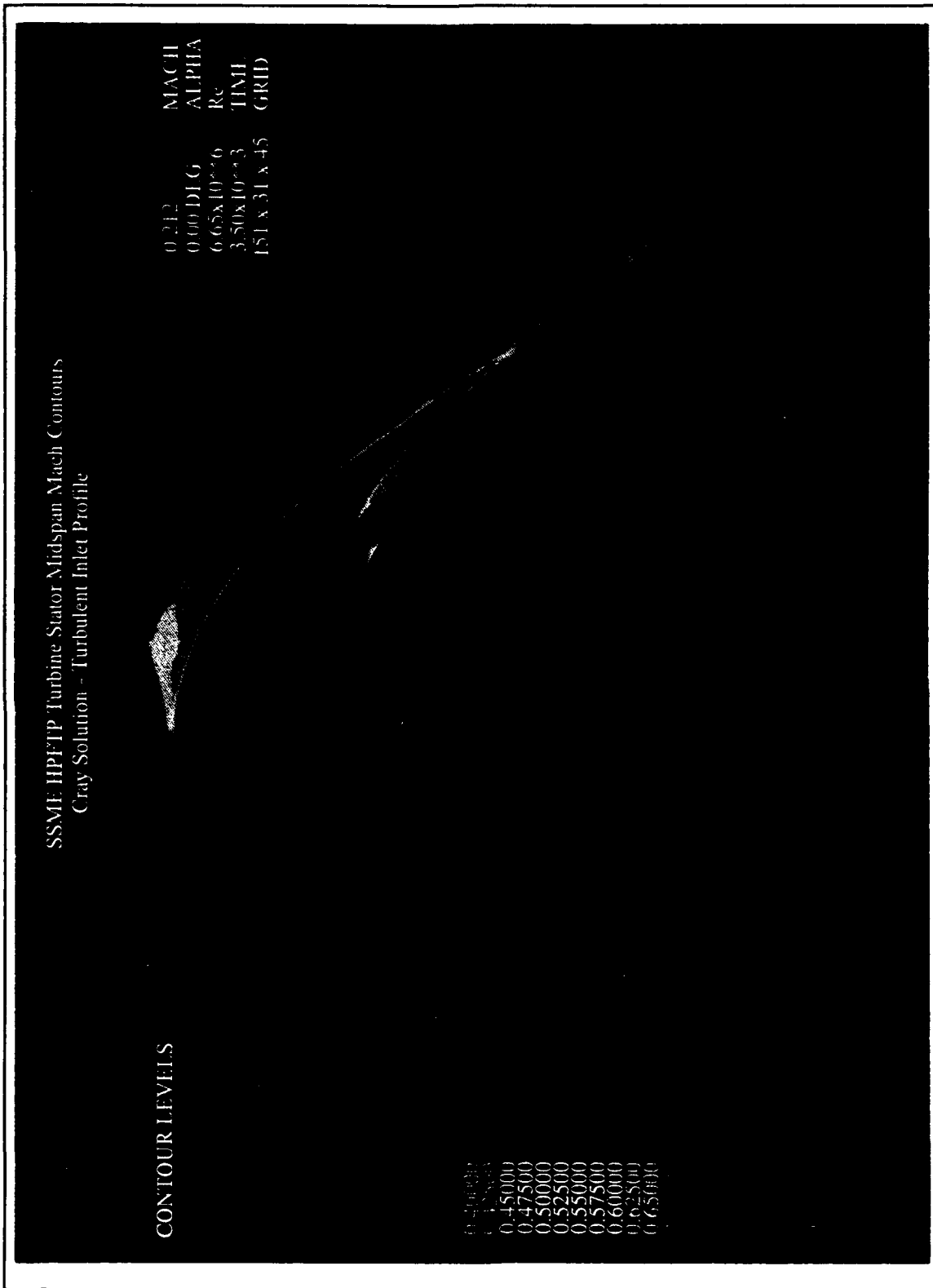


Figure 26. Mach Contours - Cray - Turbulent

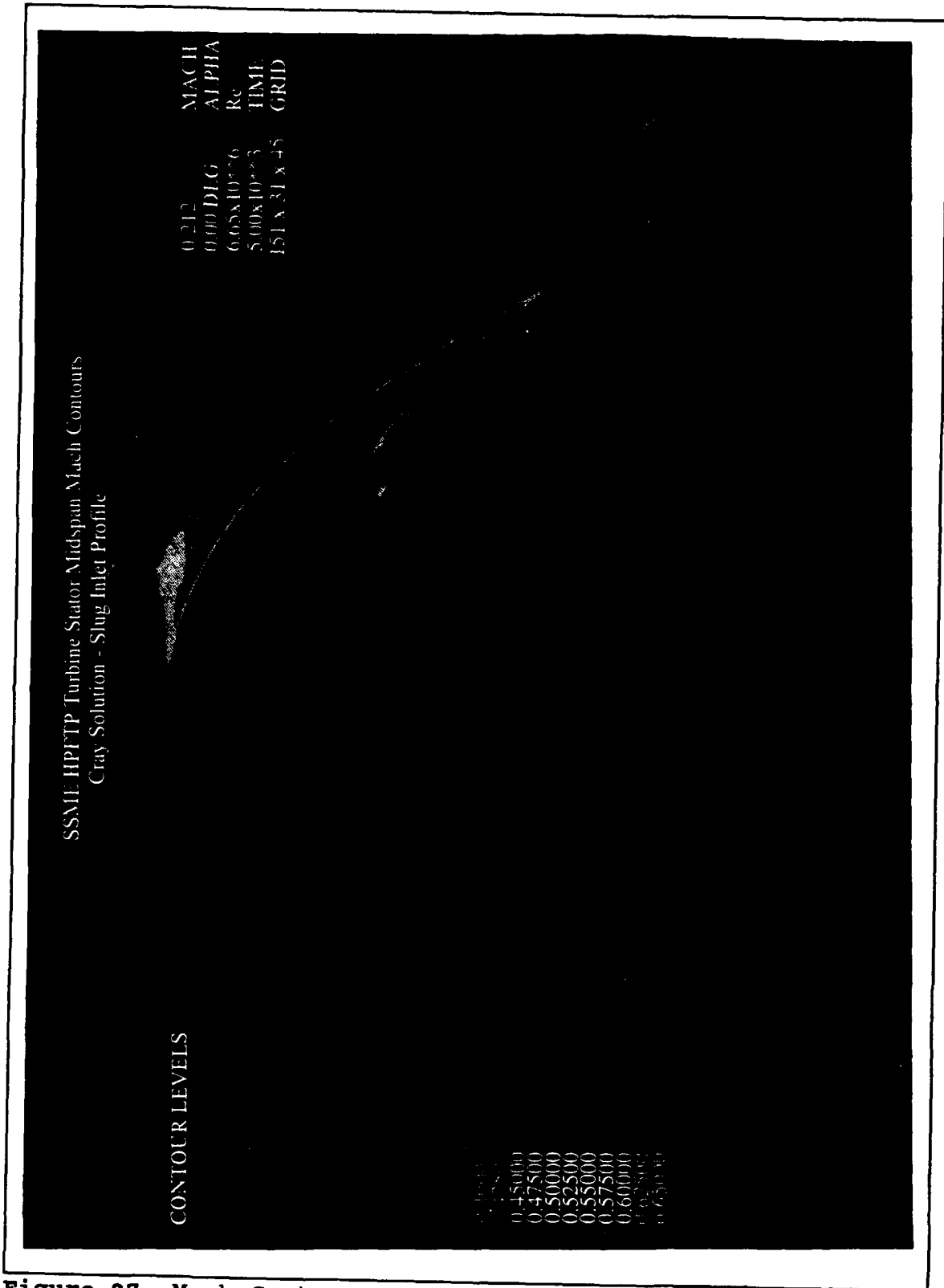


Figure 27. Mach Contours - Cray - Slug Flow

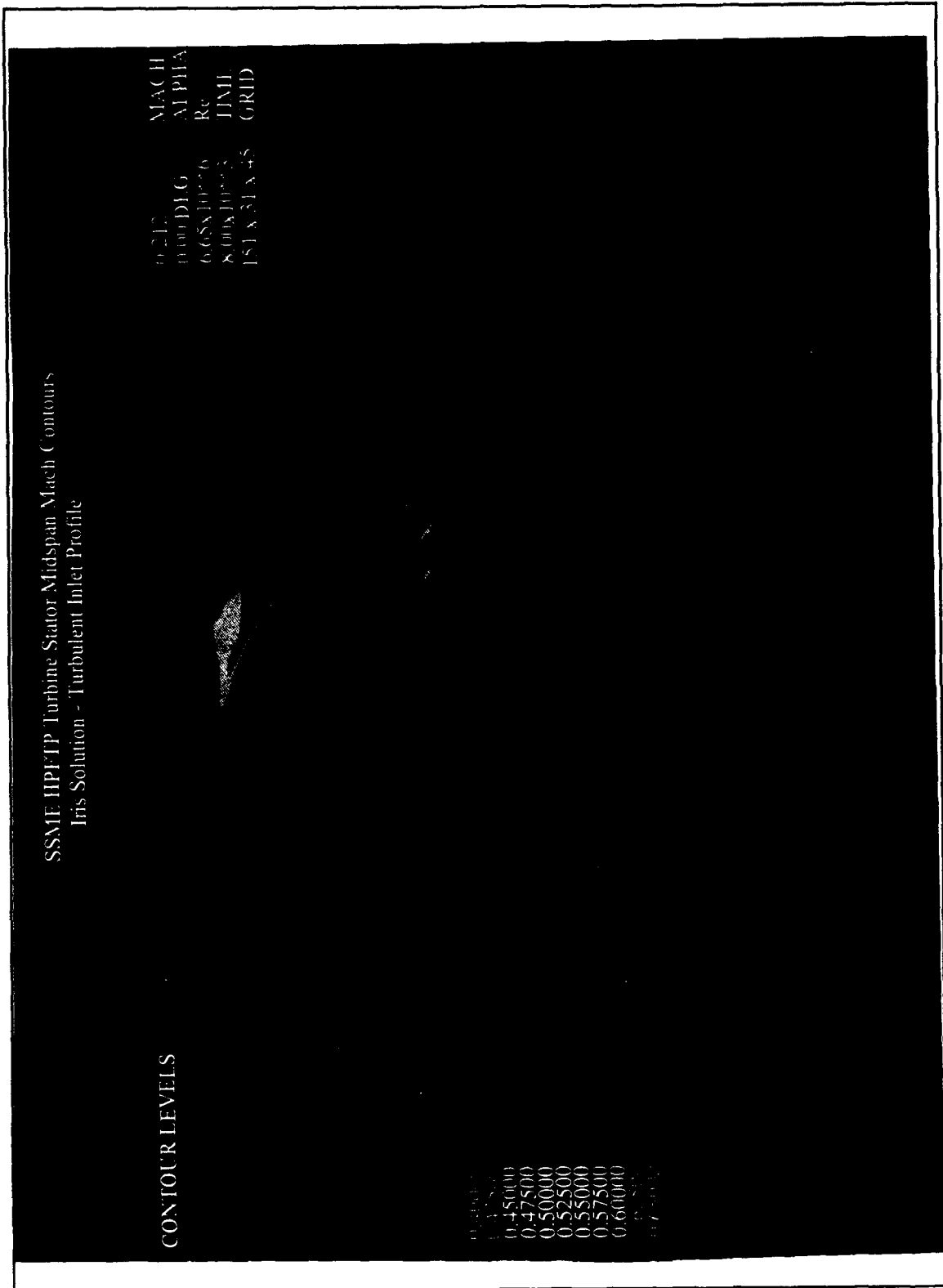


Figure 28. Mach Contours - Iris - Turbulent

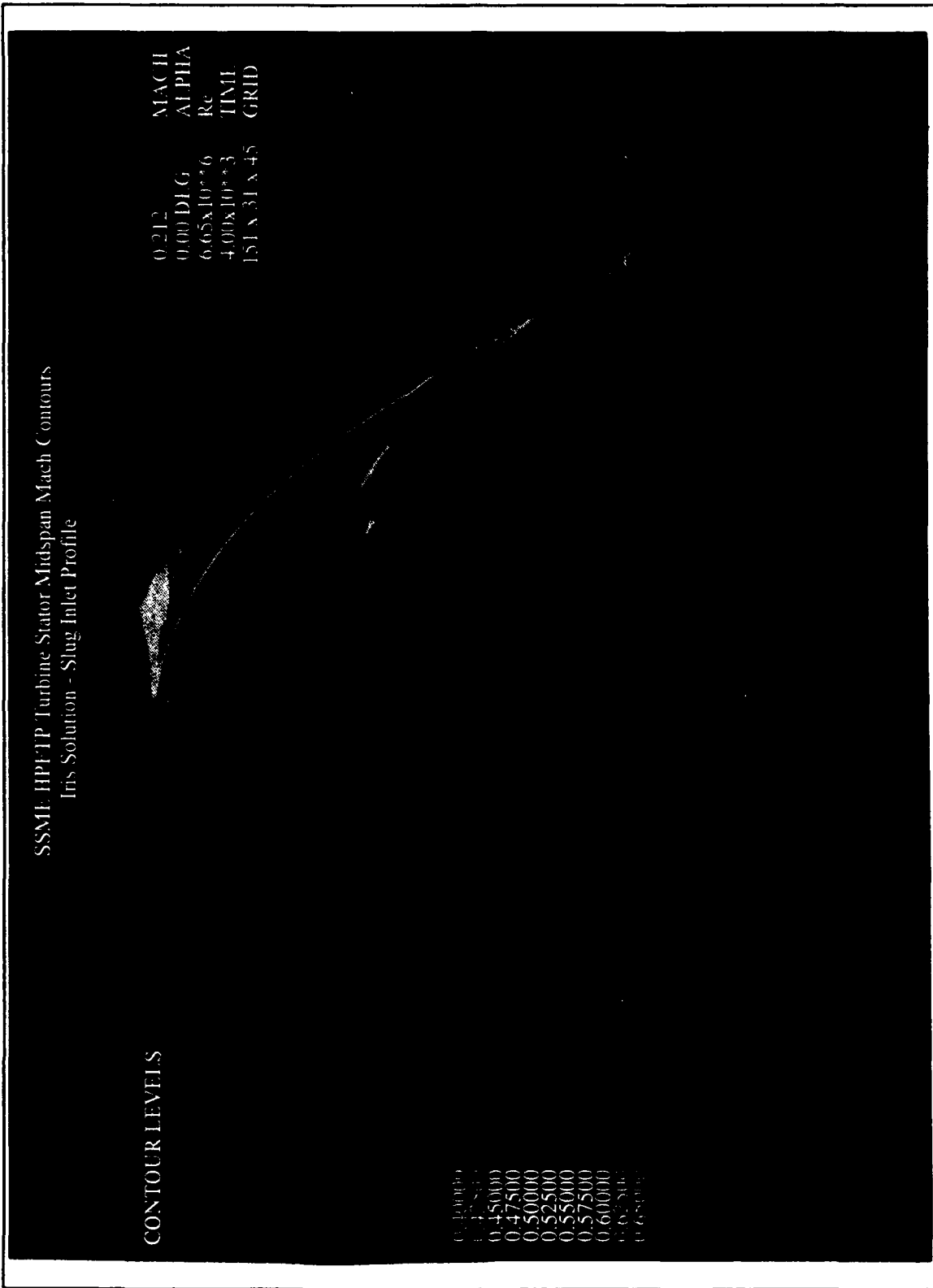


Figure 29. Mach Contours - Iris - Slug Flow

fact that the wake does not follow this cut indicates that the solution is somewhat independent of grid geometry and that continuity is satisfied at each point in the flow.

Figures 30 through 33 the total pressure contours across the exit plane of the stator. These plots are also nearly identical but small variations do exist in the upper left corner of the exit plane. The turbulent solutions, Figures 30 and 32, are different in this region from the slug flow solutions, Figures 31 and 33. This would indicate that the solution is somewhat dependent on inlet velocity profile.

In these figures, it is also possible to see the variation in wake location along the span. The yellow area at the edges of the plots shows that the wake bows toward the pressure side at midspan. This may be explained by the bowed shape of the trailing edge of the stator. As the flow turns around the stator, the extended arclength along the surface in the region of the midspan may turn the flow farther than the shorter arclength along the stator at the hub and tip.

In the boundary layer at the hub there is a small region of blue and yellow in the area of the grid cut. Although not a discontinuity, this locus coincident with the grid cut may indicate some solution dependence on grid geometry.

An example of the residual histories of two solutions is shown in Figure 34. The plot shows that the residuals matched exactly for the first 3500 iterations. The Iris

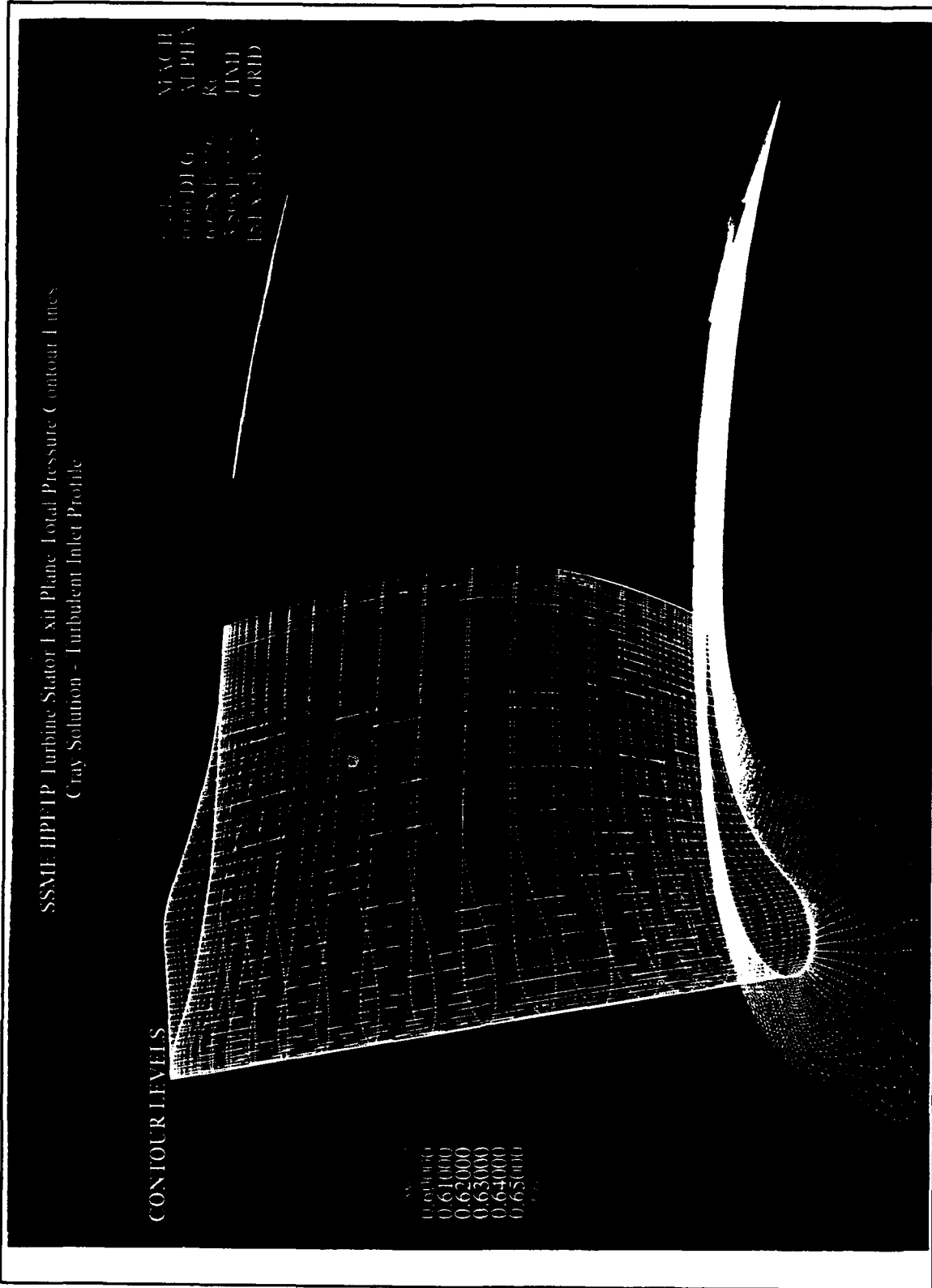


Figure 30. Total Pressure - Cray - Turbulent

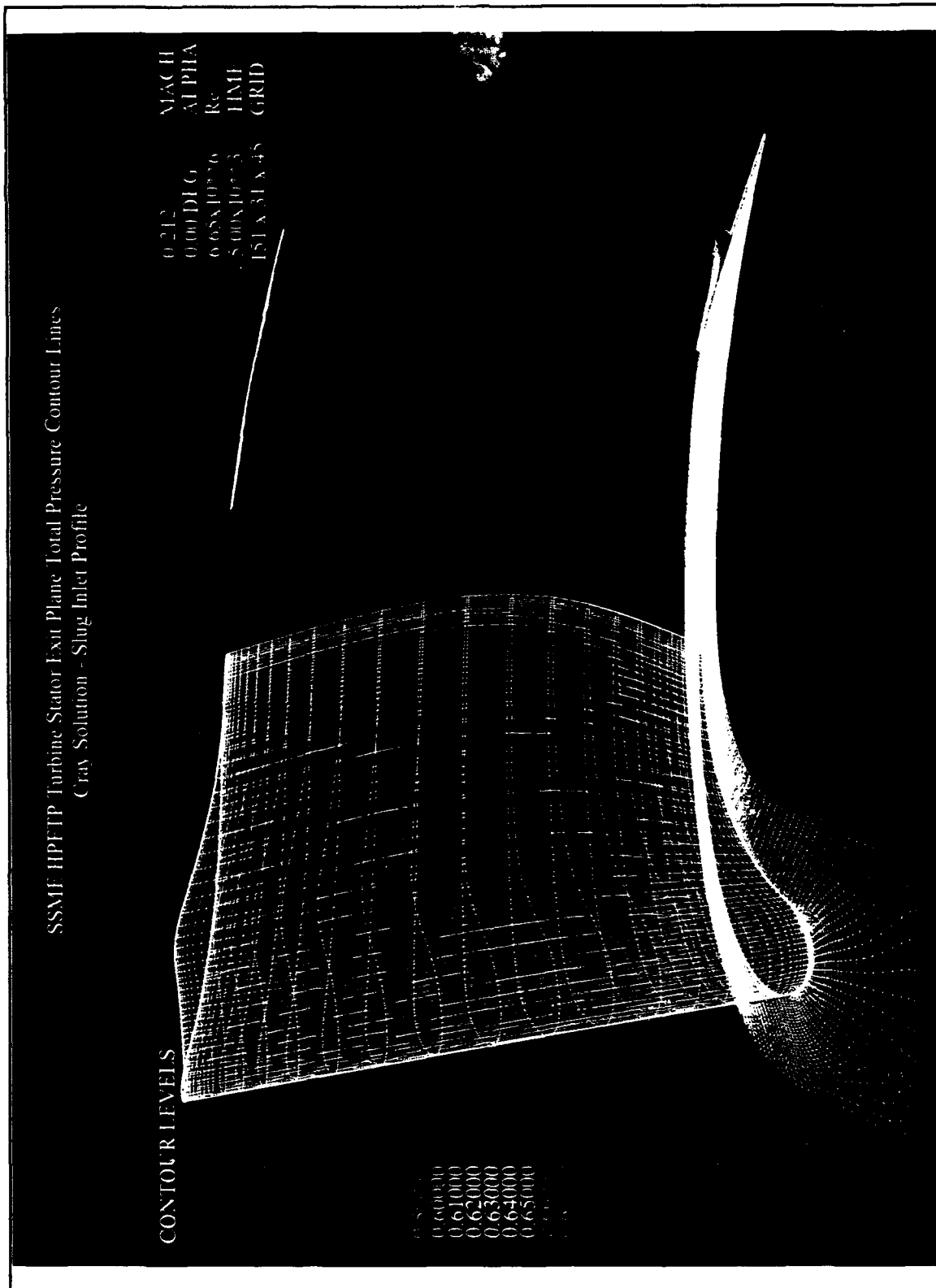


Figure 31. Total Pressure - Cray - Slug Flow

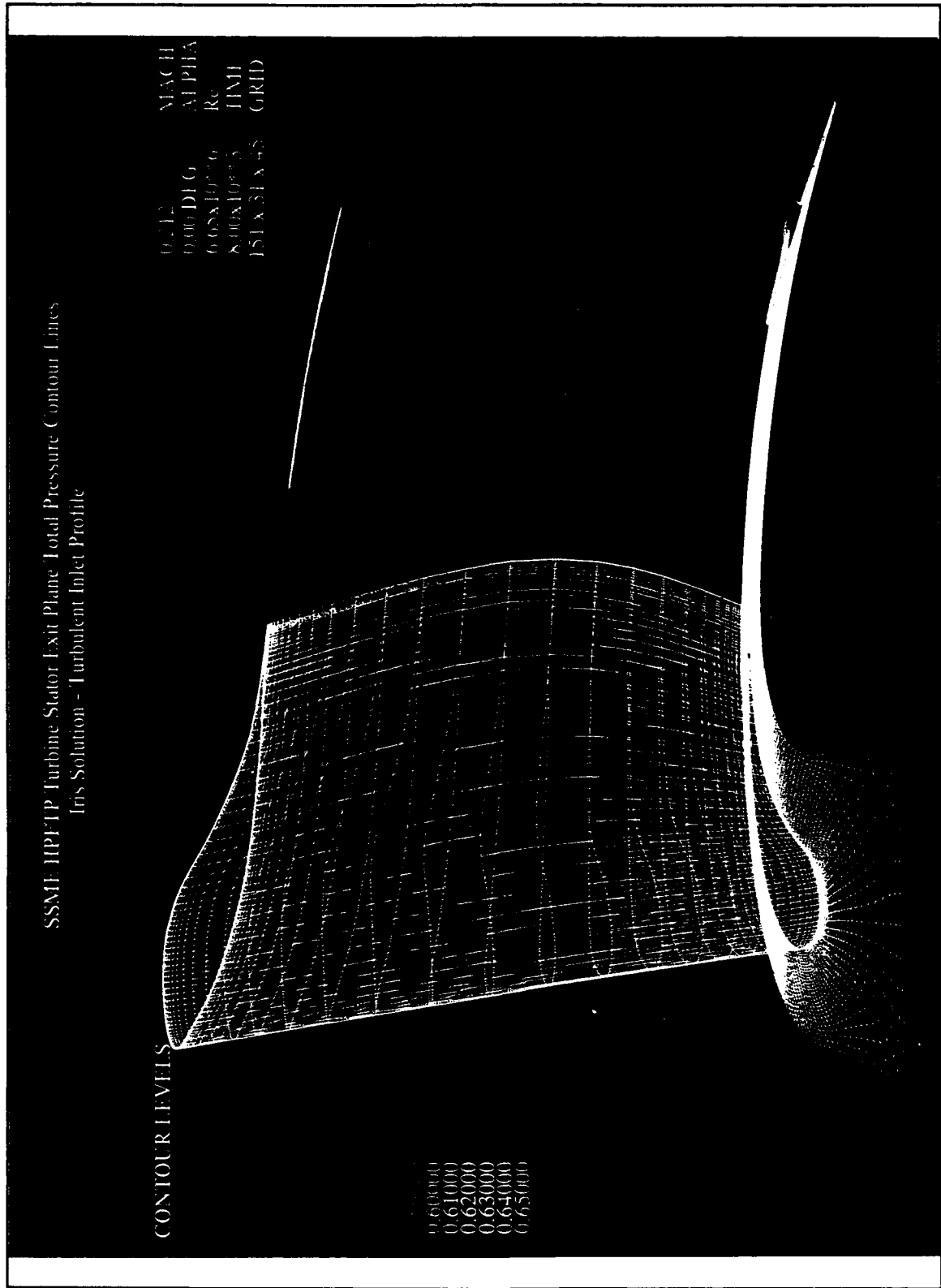


Figure 32. Total Pressure - Iris - Turbulent

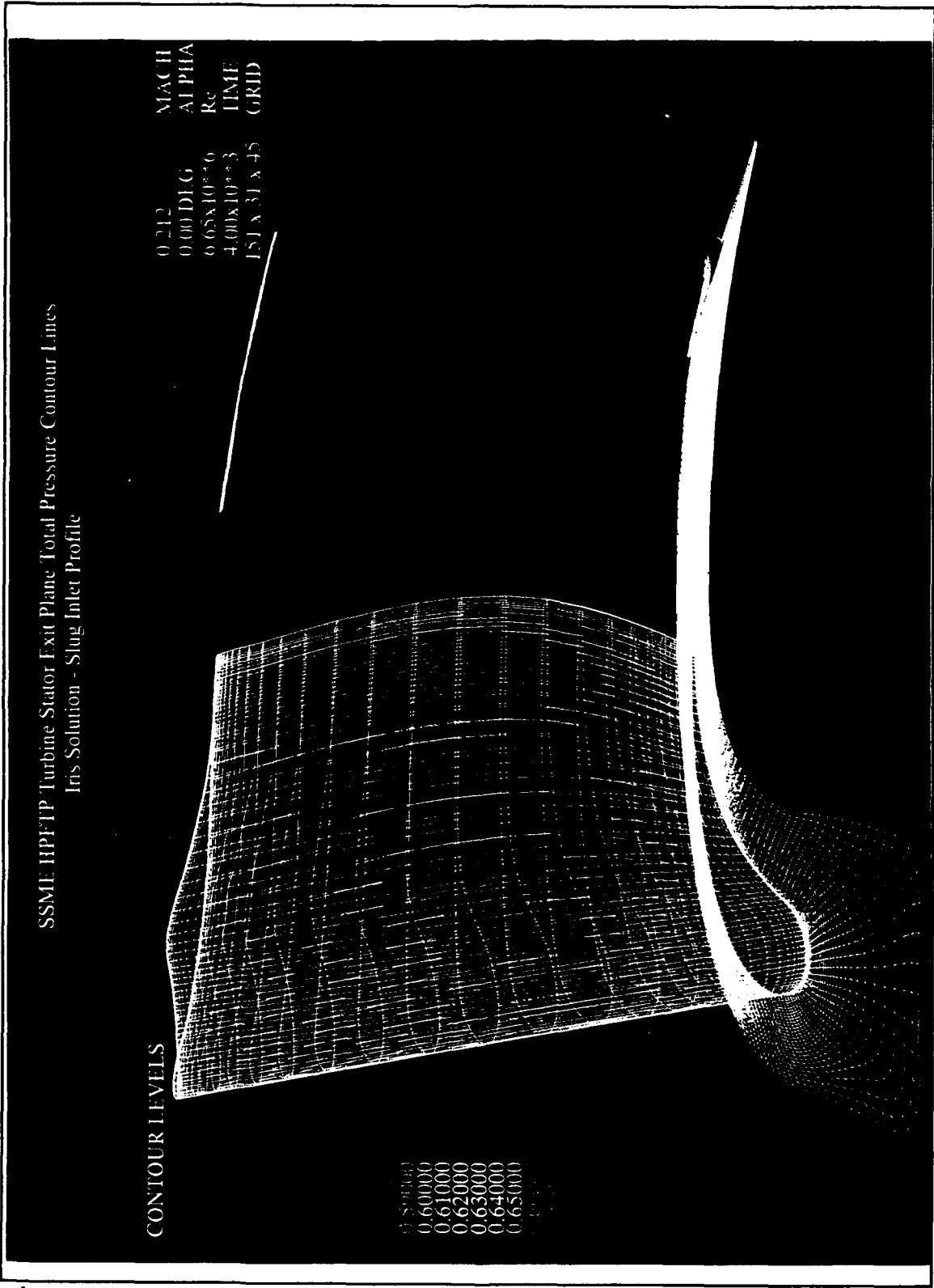


Figure 33. Total Pressure - Iris - Slug Flow

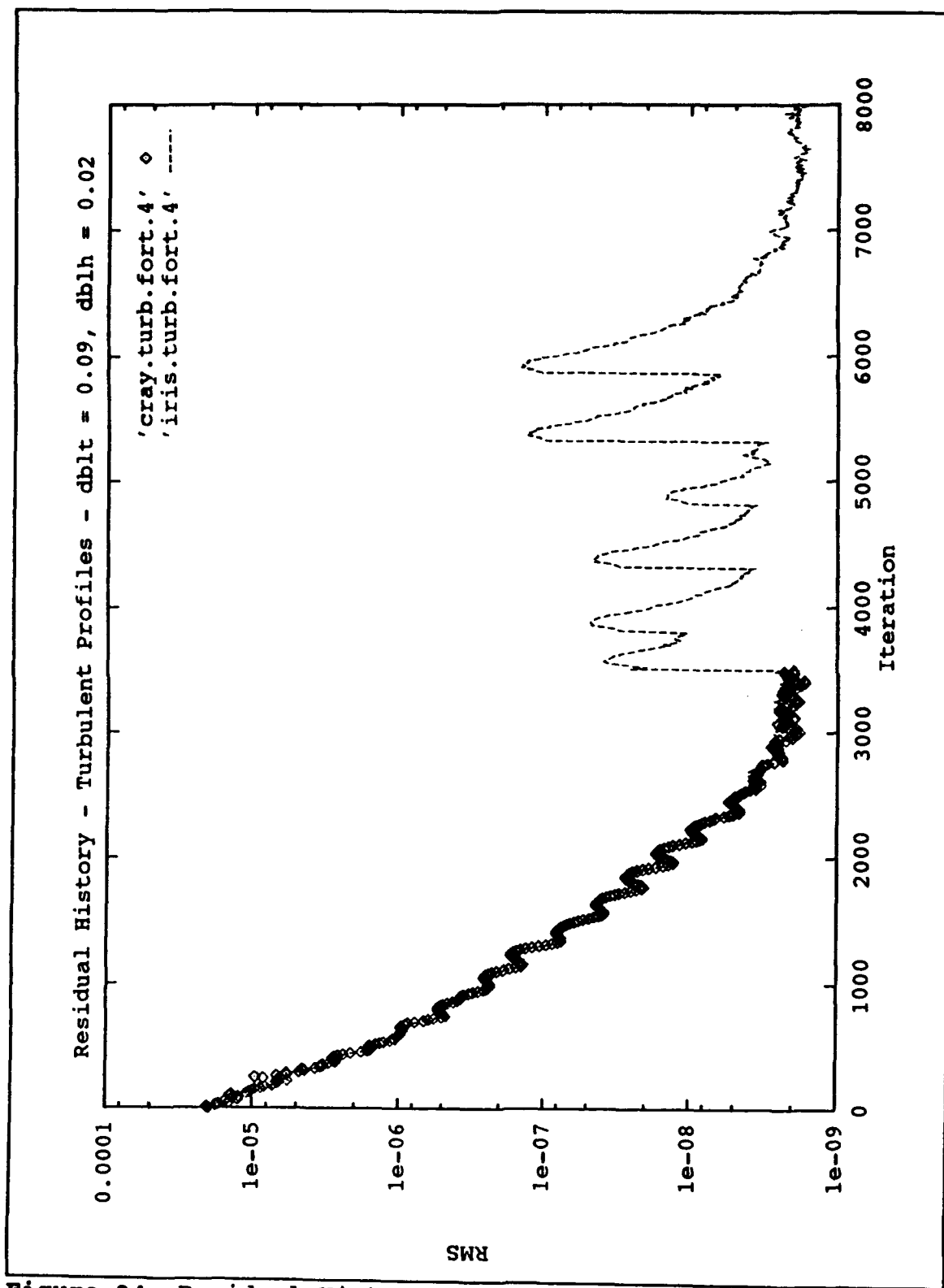


Figure 34. Residual History Example

solution was continued beyond 3500 iterations in order to see the effect of varying the inlet velocity profile. Each of the variations of the input file is marked by a significant rise in residuals. However, after approximately 500 iterations each solution converged to nearly the same residual value. Even after seven changes in the input file to vary the inlet velocity profile, the residuals converged to four orders of magnitude below their start. This shows that the solution with the input grid generated by TCGRID is very stable.

VI. CONCLUSIONS AND RECOMMENDATIONS

A. EXPERIMENT

A working test model of the first stage of the SSME HPFTP ATD turbine has been put into operation in the Naval Postgraduate School's Turbine Test Rig (TTR). The TTR subsystems have been successfully exercised; however, all lines and connections should be inspected, cleaned and repaired as necessary before any measurements are taken for performance evaluation. Connections should be completed to the water temperature probes and torque meter on the dynamometer and data acquisition should be automated. Three methods of calculating the power out of the turbine should be automated and output on-line: namely, using the flow rate and stagnation temperature drop of the air through the turbine, using flow rate and temperature rise of the water in the dynamometer, and using the rotational speed and torque generated in the dynamometer. Once the system alignment is verified, the shroud inserts should be installed and the performance measured.

The inlet flow circumferential uniformity should be checked. If the flow is not uniform, a flow straightener should be designed and inserted into the inlet duct. It is

also recommended that the inlet and exit velocity profiles be determined experimentally .

Ultimately, the turbine outer casing will need to be modified to allow LDV measurements of the flow, particularly in the tip clearance region.

B. NUMERICAL SIMULATION

A working CFD model of the SSME HPFTP ATD turbine first stage stator has been generated. Four solutions were generated on two different computers. It is recommended that more work be done to investigate the inlet-velocity profile dependence on the computer system, as this is not acceptable. An investigation is needed to determine whether the anomaly at the grid cut on the hub is grid dependent, or is a real, physical phenomenon.

In order to yield more realistic flow solutions, the inlet struts that hold the bullet nose upstream of the first-stage stator should be modeled so that their effect can be included in the flow solution. Computations can be made with input of the actual inlet velocity profile, once this has been determined experimentally. For an analysis of the complete stage, the rotor geometry must yet be modeled. Such a modeling of the downstream portions of the turbine will allow comparison with experimental results when the turbine is tested with the rotor clearance at the design value.

APPENDIX A. ENGINEERING DRAWINGS

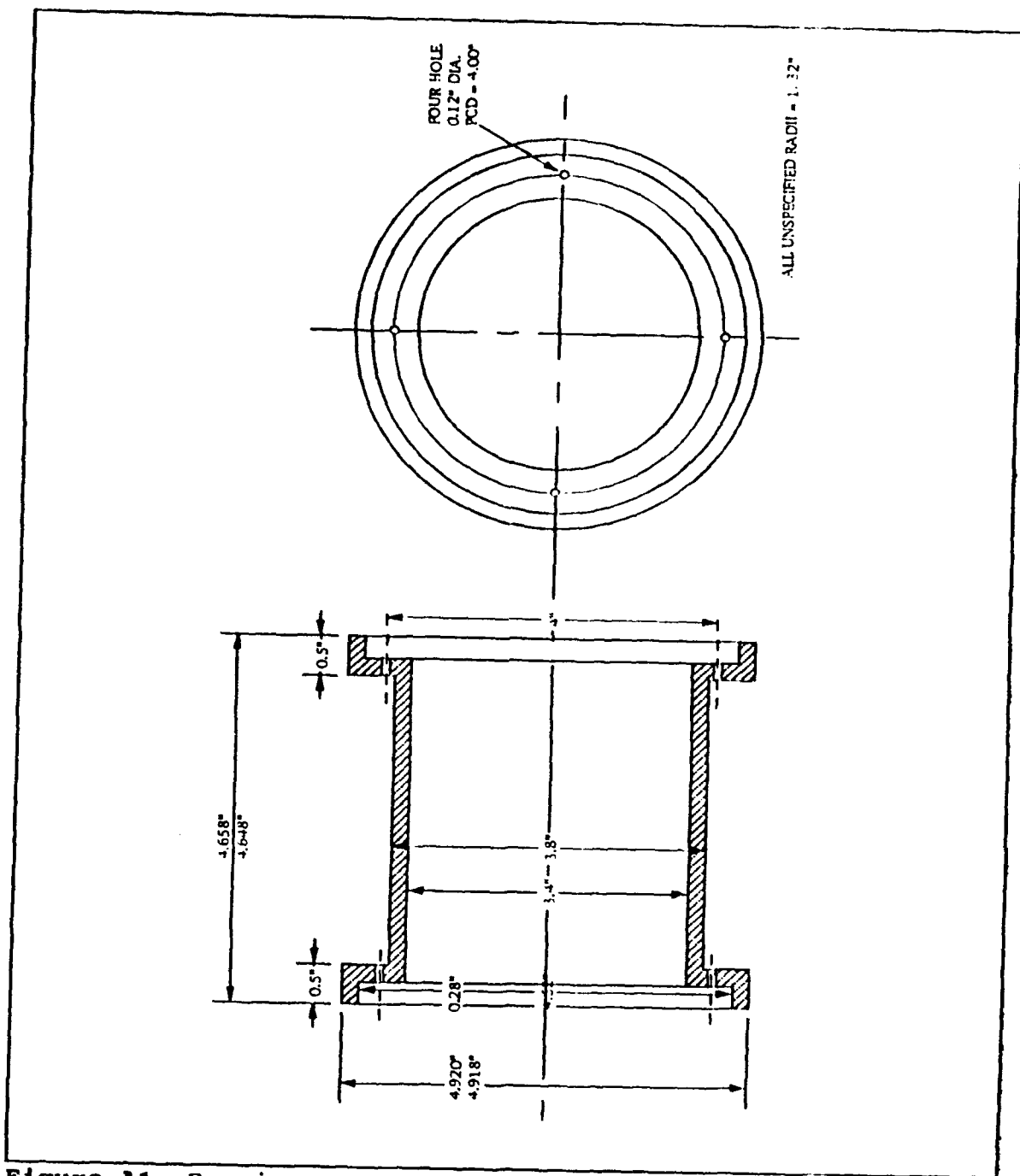
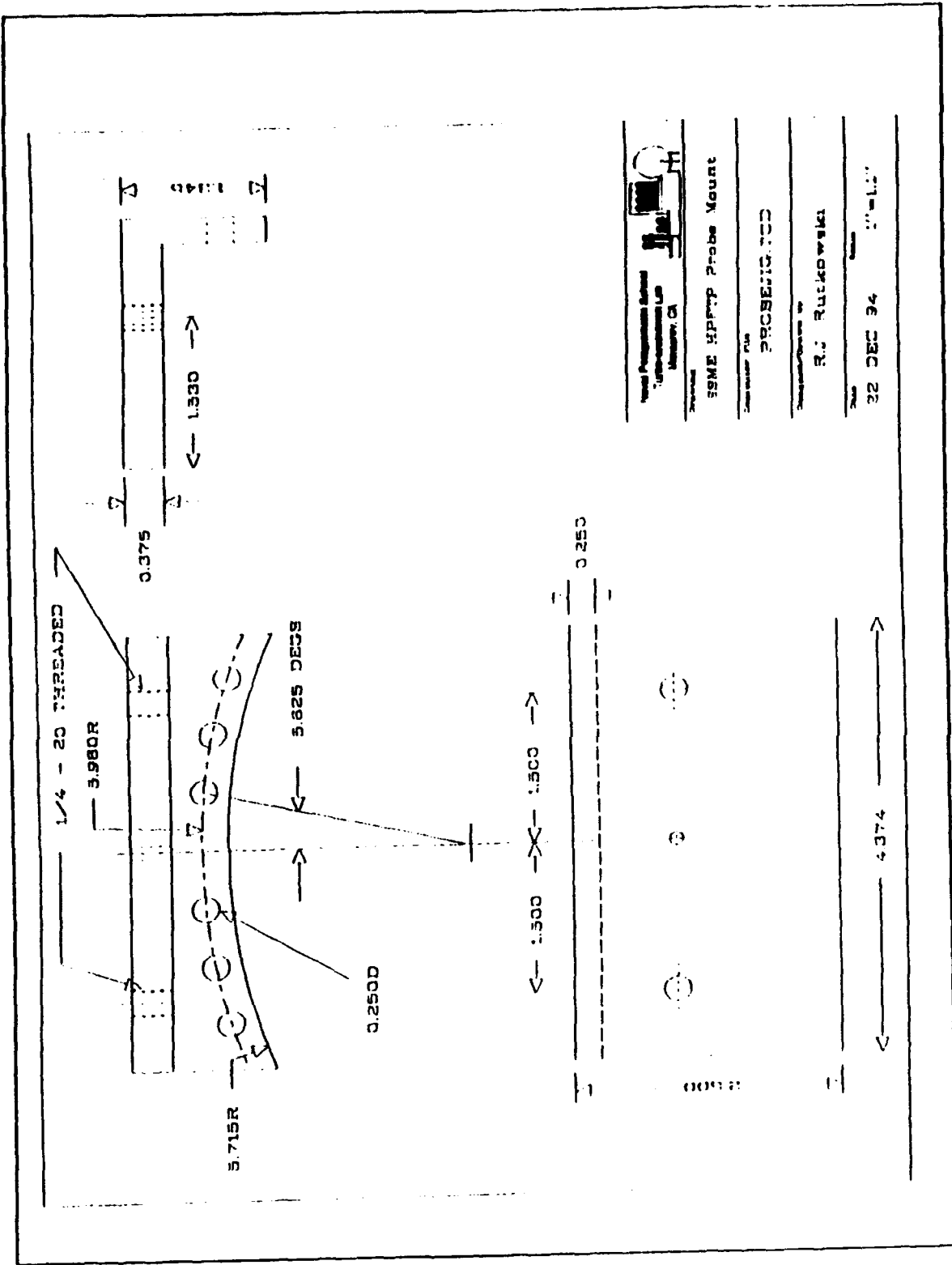


Figure A1. Bearing Outer Spacer



Westinghouse Electric
 Instrumentation Lab
 Baltimore, MD

SSME HP/TP Probe Mount

PROJECT: 100

R. J. Rutkowski

32 DEC 84

Figure A2. Probe Mount

APPENDIX B. CALCULATIONS

A. MASS FLOW RATE

The following assumes the 9.0 in. orifice is installed and is derived from Vavra [Ref. 16].

First solve:

$$\dot{m}' = c\alpha Y_1 \zeta \sqrt{\frac{P_1 h_w}{T_1}} \quad \text{with } \zeta = 1;$$

$$\dot{m}' = c\alpha Y_1 \sqrt{\frac{P_1 h_w}{T_1}}$$

Now find;

$$x = 0.2525 \frac{\dot{m}'}{z}$$

where,

$$z = 1.9 + 0.24 \left(\frac{t_1}{100} - 1 \right)$$

$$\zeta = f(x)$$

$$\dot{m} = \zeta \dot{m}' \quad \text{in lbm/s.}$$

t_1 = temperature ahead of orifice ($^{\circ}\text{F}$)

h_w = pressure drop across orifice (in. H_2O)

P_1 = absolute pressure ahead of orifice (in. Hg)

1. Flange Taps

$$\dot{m}' = c\alpha Y_1 \sqrt{\frac{P_1 h_w}{T_1}}$$

where $T_1 = t_1 + 460$.

Therefore,

$$\dot{m}' = 6.6445 \left[1 + 0.0015 \frac{(t_1 - 60)}{100} \right] \left(1 - 0.027 \frac{h_w}{P_1} \right) \sqrt{\frac{P_1 h_w}{t_1 + 460}}$$

$$z = 1.9 + 0.24 \left(\frac{t_1}{100} - 1 \right)$$

$$x = 0.2525 \frac{\dot{m}'}{z}$$

$$\zeta = 1 + \frac{0.0047}{x}$$

$$\dot{m} = \zeta \dot{m}'.$$

2. Vena Contracta Taps

$$\dot{m}' = 6.7720 \left[1 + 0.0015 \frac{(t_1 - 60)}{100} \right] \left(1 - 0.027 \frac{h_w}{P_1} \right) \sqrt{\frac{P_1 h_w}{t_1 + 460}}$$

$$z = 1.9 + 0.24 \left(\frac{t_1}{100} - 1 \right)$$

$$x = 0.2525 \frac{\dot{m}'}{z}$$

$$\zeta = 1 + \frac{0.0029}{x}$$

$$\dot{m} = \zeta \dot{m}'.$$

B. TURBINE POWER

$$\text{Power} = \dot{m} C_p \Delta T$$

$C_p = 0.24$ Btu/lbm. \cdot R for air.

$$\Delta T = TT_3 - TT_4$$

TT_4 = Stagnation Temperature of Air at Turbine Exit ($^{\circ}$ F)

TT_3 = Stagnation Temperature of Air at Turbine Entrance ($^{\circ}$ F)

Since 1 Hp \cdot s = 550 ft.lbf and 778 ft.lbf = 1 BTU,

$$\text{Power} = \dot{m} \cdot 0.24 (TT_3 - TT_4) \frac{778}{550}.$$

C. TURBINE EFFICIENCY

$$\text{Efficiency} = \frac{TT_3 - TT_4}{TT_3 - TT_{4i}}$$

where TT_{4i} = Isentropic stagnation temperature is given by

$$TT_{4i} = TT_3 \left(\frac{PT_4}{PT_3} \right)^{\frac{\gamma-1}{\gamma}}.$$

APPENDIX C. COMPLETE TABLE OF MEASUREMENTS

TTR Data

Speed RPM	TT2 (°F)	PT2 (in. Hg)	TT3 (°F)	PT3 (in. Hg)	TT4 (DEG. F)	PT4 (in. Hg)	Vena P31 (in. H2O)	Contracta P34 (in. H2O)	Pressure Difference (in. H2O)
880	34	0	81	0.4	77	0.05	25.0625	38.75	-12.6875
1420	31	0	88	0.5	84	0.1	37.125	37.75	5.375
1550	34	0	92	0.85	86	0.15	28.25	37.25	-9
2100	55	0	94	1.5	87	0.25	18.125	43.375	-25.25
3700	99	0.05	97	4.8	94	0.75	22.125	40.5	-18.375
5950	107	0.15	105	12.7	76	2	25.25	38.75	-13.5
7900	112	0.2	111	19.3	71	2.6	15	41.875	-29.875

Speed RPM	Flange P22 (in. H2O)	Taps P33 (in. H2O)	Pressure Difference (in. H2O)	"Dump" Valve Position	"Eject" Valve Position	"Comb" Valve Position	Discharge Pressure (PSIG)	TTR TUR Accel	Bearing T4 (°F)	Bearing T5 (°F)
880	0	0	0	10	2	10	3.6	0.007	57	55
1420	38.5	20.0625	18.4375	0	2	10	4.2	0.027	72	72
1550	38.75	19.75	19	0	2	8	4.4	0.029	77	73
2100	37.5	20.875	16.625	0	2	6	5.6	0.026	79	82
3700	40.825	16.125	24.5	0	2	4	11.4	0.035	82	94
5950	45.5	11.75	33.75	0	6	4	9.6	0.12	89	88
7900	37.875	19.8125	17.375	0	9	3.5	12.3	0.15	94	85

APPENDIX D. FORTRAN PROGRAM AND INPUT FILES

RVC3D Input File

```
-----  
'SSME HPFTP -- Indigo -- Real Slug Flow'  
&n11 im=151 jm=31 km=45 itl=20 iil=70 &end  
&n12 cfl=4.0 avisc1=0.0 avisc2=0.5 avisc4=1.5 ivdt=1 nstg=4  
itmax=985  
irs=1 epi=0.50 epj=0.60 epk=0.60 &end  
&n13 ibcin=3 ibcex=3 isymt=0 ires=1 icrnt=50  
iresti=1 iresto=1 ibcpw=0 iqin=0 &end  
&n14 emxx=0.212 emty=0.0 emrz=0.0 expt=0.0 prat=0.6500  
ga=1.4  
om=0.000000 igeom=1 alex=-60.0 &end  
&n15 ilt=2 tw=1.00 renr=6.651e6 prnr=.7 prtr=.9  
vispwr=.666666  
srtip=0.0 cmutm=14. jedge=15 kedge=11 iltin=0 dblh=0.00  
dblt=0.00 &end  
&n16 io1=1 io2=151 oar=0. ixjb=0 njo=1 nko=3  
jo=1 ko=13 17 21 &end  
-----
```

Inlet.f - Reads RVC3D output and builds files for plotting
 Inlet Velocity Profiles.

```

c*****
c  inlet.f reads rvc3d files & writes ascii files for
plotxy
c  unit 1 = input xyz file (fort.1)
c  unit 3 = input q file (fort.3)
c  unit 17 = output inlet velocity profiles
c  unit 4 = output residual history
c*****
parameter (ni=152,nj=32,nk=46)
real x(ni,nj,nk),y(ni,nj,nk),z(ni,nj,nk)
real qq(5,ni,nj,nk),resd(5000,5)
real vel(5),zz(5)
dimension ii(5)
c  i-values are hard-wired below
data ii/60,70,75,80,90/
c*****
c  read grid coordinates
c*****
read(1,*)im,jm,km
read(1,*)((x(i,j,k),i=1,im),j=1,jm),k=1,km),
1 ((y(i,j,k),i=1,im),j=1,jm),k=1,km),
2 ((z(i,j,k),i=1,im),j=1,jm),k=1,km)
c*****
c  read restart file

*****
read(3,*)imax,jmax,kmax
read(3,*)fsmach,alpha,re,time
c
  icheck=iabs(im-imax)+iabs(jm-jmax)+iabs(km-kmax)
  if(icheck.ne.0)then
    write(6,610)im,jm,km,imax,jmax,kmax
    stop
  endif
c
read(3,*)((qq(l,i,j,k),i=1,im),j=1,jm),k=1,km),l=1,5)
c
c  additional residual data
read(3,*)itl,iil,phdeg,ga,om,nres,dum,dum,dum,dum
read(3,*)((resd(nr,l),nr=1,nres),l=1,5)
c*****
c  vel to unit 17
c*****
itr=im+1-itl
ggm=ga*(ga-1.)
j= jm
c  normalize x by chord

```

```

c      do 7 l=1,5
c      k=kk(l)
c      xmin=x(im/2,j,k)
c      xmax=x(itl,j,k)
c      do 5 i=itl,itr
c      xmin=min(xmin,x(i,j,k))
c      5 xmax=max(xmax,x(i,j,k))
c      chord=xmax-xmin
c      do 7 i=itl,itr
c      7 x(i,j,k)=(x(i,j,k)-xmin)/chord
c
c      i=75
c      j=jm
c      k=km/2
c      velinf=sqrt((qq(2,i,j,k)**2+qq(3,i,j,k)**2
c      1+qq(4,i,j,k)**2)/qq(1,i,j,k))
c
c      write(7,305)(kk(l),l=1,5)
c      do 20 k=1,km
c      do 10 l=1,5
c      i=ii(l)
c      vel(l)=sqrt((qq(2,i,j,k)**2+qq(3,i,j,k)**2
c      1+qq(4,i,j,k)**2)/qq(1,i,j,k))
c      10 zz(l)=z(i,j,k)
c      20 write(17,300)i,(zz(l),vel(l)/velinf,l=1,5)
c*****
c*****
c      300 format(i5,10f10.5)
c      305 format('  k=',5(17x,i3))
c      610 format(' ***** warning *****',/,
c      1      ' im, jm, km, read from input',3i5,' do not
match',/,
c      2      ' im, jm, km, read from restart file',3i5)
c      stop
c      end

```

```

program shrink99
*
* This inputs data and multiplies it by 0.99 for a 99%
* shrink factor.
*
real x(988),p(988)
open (unit=2,file='hotlv.dat',status='old')
open (unit=15,file='lv.tcgin',status='new')
  read(2,*) (x(i),i=1,988)
do 20 i=1,988
  p(i)=x(i)*0.99
20 continue

*
* -- print the data out in blocks
*
write (15,*) (p(i),i=1,88)
write (15,*)
write (15,*) (p(i),i=89,176)
write (15,*)
write (15,*) (p(i),i=177,264)
write (15,*)
write (15,*) (p(i),i=265,352)
write (15,*)
write (15,*) (p(i),i=353,405)
write (15,*)
write (15,*) (p(i),i=406,458)
write (15,*)
write (15,*) (p(i),i=459,511)
write (15,*)
write (15,*) (p(i),i=512,564)
write (15,*)
write (15,*) (p(i),i=565,617)
write (15,*)
write (15,*) (p(i),i=618,670)
write (15,*)
write (15,*) (p(i),i=671,723)
write (15,*)
write (15,*) (p(i),i=724,776)
write (15,*)
write (15,*) (p(i),i=777,829)
write (15,*)
write (15,*) (p(i),i=830,882)
write (15,*)
write (15,*) (p(i),i=883,935)
write (15,*)
write (15,*) (p(i),i=936,988)
end

```

TCGRID Input File

Dec 17 1993 09:43:52		grid4.in	Page 1
name	tcgrid		
name2	tcgrid		
name3	tcgrid		
name4	tcgrid		
name5	tcgrid		
name6	tcgrid		
name7	tcgrid		
name8	tcgrid		
name9	tcgrid		
name10	tcgrid		
name11	tcgrid		
name12	tcgrid		
name13	tcgrid		
name14	tcgrid		
name15	tcgrid		
name16	tcgrid		
name17	tcgrid		
name18	tcgrid		
name19	tcgrid		
name20	tcgrid		
name21	tcgrid		
name22	tcgrid		
name23	tcgrid		
name24	tcgrid		
name25	tcgrid		
name26	tcgrid		
name27	tcgrid		
name28	tcgrid		
name29	tcgrid		
name30	tcgrid		
name31	tcgrid		
name32	tcgrid		
name33	tcgrid		
name34	tcgrid		
name35	tcgrid		
name36	tcgrid		
name37	tcgrid		
name38	tcgrid		
name39	tcgrid		
name40	tcgrid		
name41	tcgrid		
name42	tcgrid		
name43	tcgrid		
name44	tcgrid		
name45	tcgrid		
name46	tcgrid		
name47	tcgrid		
name48	tcgrid		
name49	tcgrid		
name50	tcgrid		
name51	tcgrid		
name52	tcgrid		
name53	tcgrid		
name54	tcgrid		
name55	tcgrid		
name56	tcgrid		
name57	tcgrid		
name58	tcgrid		
name59	tcgrid		
name60	tcgrid		
name61	tcgrid		
name62	tcgrid		
name63	tcgrid		
name64	tcgrid		
name65	tcgrid		
name66	tcgrid		
name67	tcgrid		
name68	tcgrid		
name69	tcgrid		
name70	tcgrid		
name71	tcgrid		
name72	tcgrid		
name73	tcgrid		
name74	tcgrid		
name75	tcgrid		
name76	tcgrid		
name77	tcgrid		
name78	tcgrid		
name79	tcgrid		
name80	tcgrid		
name81	tcgrid		
name82	tcgrid		
name83	tcgrid		
name84	tcgrid		
name85	tcgrid		
name86	tcgrid		
name87	tcgrid		
name88	tcgrid		
name89	tcgrid		
name90	tcgrid		
name91	tcgrid		
name92	tcgrid		
name93	tcgrid		
name94	tcgrid		
name95	tcgrid		
name96	tcgrid		
name97	tcgrid		
name98	tcgrid		
name99	tcgrid		
name100	tcgrid		

Dec 17 1993 09:43:52		grid4.in	Page 2
name101	tcgrid		
name102	tcgrid		
name103	tcgrid		
name104	tcgrid		
name105	tcgrid		
name106	tcgrid		
name107	tcgrid		
name108	tcgrid		
name109	tcgrid		
name110	tcgrid		
name111	tcgrid		
name112	tcgrid		
name113	tcgrid		
name114	tcgrid		
name115	tcgrid		
name116	tcgrid		
name117	tcgrid		
name118	tcgrid		
name119	tcgrid		
name120	tcgrid		
name121	tcgrid		
name122	tcgrid		
name123	tcgrid		
name124	tcgrid		
name125	tcgrid		
name126	tcgrid		
name127	tcgrid		
name128	tcgrid		
name129	tcgrid		
name130	tcgrid		
name131	tcgrid		
name132	tcgrid		
name133	tcgrid		
name134	tcgrid		
name135	tcgrid		
name136	tcgrid		
name137	tcgrid		
name138	tcgrid		
name139	tcgrid		
name140	tcgrid		
name141	tcgrid		
name142	tcgrid		
name143	tcgrid		
name144	tcgrid		
name145	tcgrid		
name146	tcgrid		
name147	tcgrid		
name148	tcgrid		
name149	tcgrid		
name150	tcgrid		
name151	tcgrid		
name152	tcgrid		
name153	tcgrid		
name154	tcgrid		
name155	tcgrid		
name156	tcgrid		
name157	tcgrid		
name158	tcgrid		
name159	tcgrid		
name160	tcgrid		
name161	tcgrid		
name162	tcgrid		
name163	tcgrid		
name164	tcgrid		
name165	tcgrid		
name166	tcgrid		
name167	tcgrid		
name168	tcgrid		
name169	tcgrid		
name170	tcgrid		
name171	tcgrid		
name172	tcgrid		
name173	tcgrid		
name174	tcgrid		
name175	tcgrid		
name176	tcgrid		
name177	tcgrid		
name178	tcgrid		
name179	tcgrid		
name180	tcgrid		
name181	tcgrid		
name182	tcgrid		
name183	tcgrid		
name184	tcgrid		
name185	tcgrid		
name186	tcgrid		
name187	tcgrid		
name188	tcgrid		
name189	tcgrid		
name190	tcgrid		
name191	tcgrid		
name192	tcgrid		
name193	tcgrid		
name194	tcgrid		
name195	tcgrid		
name196	tcgrid		
name197	tcgrid		
name198	tcgrid		
name199	tcgrid		
name200	tcgrid		

LIST OF REFERENCES

1. Studevan, C.C., "Design of a Cold-Flow Test Facility for the High-Pressure Fuel Turbopump Turbine of the Space Shuttle Main Engine," Master's Thesis, Naval Postgraduate School, Monterey, California, December 1993.
2. Gaddis, S.W., Hudson, S.T., and Johnson, P.D., "Cold Flow Testing of the Space Shuttle Main Engine Alternate Turbopump Development High Pressure Fuel Turbine Model", ASME Paper 92-GT-280, June 1992.
3. Hudson, S.T., and others, "Cold Flow Testing of the Space Shuttle Main Engine High Pressure Fuel Turbine Model", AIAA Paper 91-2503, June 1991.
4. Chima, R.V., "TCGRID (Turbomachinery C-Grid)," User's Manual, November 1990.
5. Chima, R.V., "RVC3D (Rotor Viscous Code 3-D)," User's Manual, March 1992.
6. Kane, W.J., "Experimental Investigation of the Effects of Rotor to Stator Axial Spacing on the Performance of a Single Stage Transonic Axial Turbine," Master's Thesis, Naval Postgraduate School, Monterey, California, 1978.
7. Walatka, P.P., and Buning, P.G., "PLOT3D Users Manual," NASA TM 101067, Mar 1989.
8. Sorenson, R.L., "A Computer Program to Generate Two-Dimensional Grids About Airfoils and Other Shapes by the Use of Poisson's Equation," NASA TM-81198, 1980.
9. Katsanis T., and McNally, W.D., "Revised Fortran Program for Calculating Velocities and Streamlines on the Hub-Shroud Midchannel Stream Surface of an Axial-, Radial-, or Mixed Flow Turbomachine or Annular Duct," NASA TN D- 8430, 1977.
10. Kirtley, K.R., Private Communication, 23 July 1993.
11. Chima, R.V., Private Communication, January 1994.

12. Chima, R.V., and Yokota, J.W., "Numerical Analysis of Three- Dimensional Viscous Flows in Turbomachinery," AIAA Journal, Vol. 28, No. 5, May 1990.
13. Chima, R.V., "Viscous Three-Dimensional Calculations of Transonic Fan Performance," NASA TM 103800, 1991.
14. Baldwin, B.S., and Lomax, H., "Thin-Layer Approximation and Algebraic Model for Separated Turbulent Flows," AIAA Paper 78-257, January 1978.
15. Chima, R.V., Giel, P.W., and Boyle, R.J., "An Algebraic Turbulence Model for Three-Dimensional Viscous Flows," NASA TM 105931, January 1993.
16. Vavra, M.H., "Determination of Flow Rates of Allis-Chalmers Axial Flow Compressor VA-312 of Propulsion Laboratories by Means of Square-Edged Orifices," Naval Postgraduate School TN 63T-2, 1963.

INITIAL DISTRIBUTION LIST

	No. Copies
1. Defense Technical Information Center Cameron Station Alexandria VA 22304-6145	2
2. Library, Code 052 Naval Postgraduate School Monterey CA 93943-5002	2
3. Department Chairman, AA Department of Aeronautics and Astronautics Naval Postgraduate School Monterey CA 93943	1
4. Garth V. Hobson, Turbopropulsion Laboratory Code AA/Hg Department of Aeronautics and Astronautics Naval Postgraduate School Monterey CA 93940	10
5. Naval Air Systems Command AIR-536T (Attn: Mr. Mario Duffles) Washington DC 20361-5360	1
6. Naval Air Warfare Center Aircraft Division (Trenton) PE-31 (Attn: S. Clouser) 250 Phillips Blvd Trenton NJ 08628-0176	1
7. Richard J. Rutkowski 2510 Tara Ln. South San Francisco, CA 94080	2